Optimization of Hydrogel-based Cellular Encapsulation for Diabetes Treatment

BEE 4530: Computer-Aided Engineering Applications to Biological Processes

Ed Bao, Kaavian Shariati, Nicole Alimena, Tigran Mehrabyan

Date of Submission: 5/10/18

Contents

1. Executive Summary

Cell encapsulation is an efficient and cost-effective treatment for a variety of endocrine and hormonal disorders. The use of cells to deliver therapeutics is an especially desirable means drug delivery may be achieved, and serves to eliminate issues associated with other methods of drug delivery. The application of these methods to Type 1 Diabetes is a promising area of research, and may potentially be a functional cure. As the use of cell encapsulation devices vary, the need for parameter analysis and optimization for a diabetes-focused encapsulation devices becomes apparent. More importantly, the potential complications faced by effective cell encapsulation devices must be considered in design.

The study attempted to observe the selectivity of transfer of chemical species pertinent to a pancreatic islet cell encapsulation device. The complications associated with the availability of such chemical species were also modeled with respect to variation in the parameters of the device. The Type 1 Diabetes model was designed with a cylindrical geometry, and three primary layers consisting of an islet cell containment core, a nanofiber(nylon) mesh layer, and an outer hydrogel layer. The impacts of glucose and oxygen availability on insulin secretion were of specific concern to the study. The hydrogel must be appropriately permeable to the flow of glucose, insulin, and oxygen. These concerns were addressed and studied through the use of COMSOL Multiphysics®, a commercial analysis software. A two-dimensional axisymmetric model was implemented in order to observe the diffusivity-driven mass transfer of chemical species, and their associated reactions. The computational modeling approach was chosen in order to study the effect and impact of parameter variation on the efficacy of such a device, and to computationally optimize these parameters. A steady-state study was conducted on the model with concentrations of blood glucose and oxygen as boundary conditions, as well as an insulin concentration of zero at the outermost boundary assuming total insulin removal.

Encapsulated islets under low oxygen conditions showed a loss of viable tissue, and the development of a necrotic core. Using a critical oxygen concentration of 0.001 mM in conjunction with implementing parameter variation against standard model conditions, the critical radiuses before cell death were calculated for several models. For the multiaxial transfer device, the critical radius before the presence of any cell death or necrosis was determined to be 0.00172 m after identifying the key modulator of cell life and insulin production to be oxygen. The same process was repeated with a model in which mass flux was zero at both ends of the device, resulting in a significantly lower critical radius of 0.00122m. Additionally, the computations revealed that insulin concentrations were not strongly modulated by glucose availability. The production of insulin is more heavily influenced, within the steady state conditions after a meal, by local oxygen concentrations. Iterations of the model were repeated with various hydrogels, nanofiber widths, and islet loads in order to identify gelatin as the most efficient hydrogel for insulin flux, and dispersed islets as being necessary for optimal insulin secretion. Validation of the model and results were conducted through comparison to experimental information, as well as through model C which validated the physical approximation of islets being homogeneously distributed within the core.

As the efficacy of cell-based diabetes treatments is more seriously considered, the need becomes apparent for the development of computational model such as those implemented in this study, which reveal the impacts of parameters and designs chosen on device efficiencies. Such a model may be implemented in

future research of alternate encapsulation methods for Type 1 Diabetes, as well as other disorders as they pertain to the endocrine and hormonal systems. Approaches to address these directional shifts may involve the consideration of additional parameters and domains.
Keywords: Cell Encapsulation, Diabetes, Insulin, Islet Cell, Drug Delivery

2. Introduction

2.1 Background and Literature Review

The endocrine system maintains and regulates different bodily functions through the production of hormones. Endocrine disorders involve the secretion of either too much or too little of specific hormones. The general treatment for disorders involving a *lack* of specific hormones is to replace these deficient signaling molecules. Many common endocrine disorders are due to a lack of regulation or destruction of tissues within the body [1]. Type 1 Diabetes is an example of such a disorder. Type 1 Diabetes involves a lack of Insulin (a hormone released from the pancreas) that is brought about by the destruction of pancreas cells due to the immune response [2]. Such a condition is known as an autoimmune disease, and has been diagnosed in around 1% of the population living in the United States [3]. Type 1 Diabetes leads to high blood glucose levels, and can cause frequent urination, weight loss, and excessive thirst. Further, the long-term implications of this condition involve sensational problems due to nerve damage, cardiac problems, and vision loss. Type 1 is generally diagnosed at younger ages, but can also be "late-onset" and appear at any age. Those afflicted must adopt a lifestyle that involves consistent blood glucose level monitoring and administering of insulin.

Hyperglycemia in diabetics involves an increase in blood glucose beyond normal levels due to a high intake of glucose and carbohydrates combined with a lack of efficient insulin intake. Hyperglycemia is treated by administering insulin, which helps glucose move from the blood into the cells, thus lowering blood glucose levels. Upon entering the cells, glucose is either converted to energy which is used immediately or stored as fat or glycogen until it is needed [1]. Conversely, hypoglycemia involves abnormally low glucose levels in the blood, and can be brought about when a diabetic administers too much insulin or performs physical activity without consuming an appropriate amount of carbohydrates. Hypoglycemia can cause hunger, weakness, shakiness, as well as can very quickly lead to seizures and comatosis [4].

Currently, the readily available and standard treatments for this condition are extremely tedious and only partially effective [1]. The two main aspects of the protocol for caretaking involve blood glucose testing, and administering insulin injections. Most diabetics frequently check the status of their blood sugars using fingerstick glucose testing or Continuous Glucose Monitors, which remain attached to the body. Insulin injections can be performed manually, and are generally administered through the use of a vial/syringe, multi-use "pen," or attached pump. The amount of insulin administered varies depending on how high the blood glucose levels are when tested and the amount of carbohydrates that are to be consumed [1].

Many different devices and treatment methods are currently available for use that exist within the aforementioned treatment areas, as well as other less accessible methods such as transplants. Most

recently, Freestyle's Libre system has been made available as the most modern method of continuous glucose monitoring. However, issues exist even with this new technology, as reports show this system as less accurate than other monitors that require repeated calibration. For example, when testing during periods of low blood glucose, the Libre's readings were lower than actual. Conversely, the readings were higher than actual when testing during hyperglycemia. Additionally, this device and the majority of available detection devices depend on subcutaneous sensing, which has large limitations such as a physiological lag time, local fluctuation sensitivities, and slow/variable rates [5]. Beyond these shortcomings, the use of such devices fail to relieve those afflicted with the condition from having to constantly monitor carbohydrate intakes, physical activity, and the actual use of the devices. Stem cells have been proposed as a potential answer to these shortcomings. While the research that has been conducted on the applications of stem cells for diabetic treatments is promising, many shortcomings have been witnessed in this area as well. Immune responses to implanted stem cells render the cells useless, as they may be attacked by the immune system of the body, or may be surrounded by fibroblasts through fibrosis, which completely separates the functions of the cells from the body. In order to avoid these responses, tested methods involve the need for immunosuppressant drugs to prevent rejection, which is an equally unattractive downside [6].

Cell encapsulation seeks to provide an answer to this problem and the other inefficiencies that exist in diabetes therapy. This method works through encapsulating insulin-producing islet cells with a hydrogel and nano-fiber matrix that allows for efficient insulin release and blood glucose sensing, while also allowing the transport of necessary nutrients to the cells inside. The matrix will serve to protect the stem cells from the harmful immune responses that have rendered most other implant-based diabetes therapy methods inefficient. This model will address the lack of a holistic and long-term treatment method for Type 1 Diabetes, and will incorporate several key treatment aspects (such as both efficient insulin release and glucose sensing) that in the past have only been addressed *separately* by different mechanisms. Through an analysis on mass transfer across the hydrogel and nanofiber matrix, this study will give insight into parameter optimization for cell encapsulation devices for the purposes of developing an efficient diabetes treatment method.

2.2 Problem Statement

The objective of this research was to study the applications of cell encapsulation methods to treat Type 1 Diabetes as a model condition. This involved addressing the need for more comprehensive and efficient management methods through analysis of cell encapsulation as a potential solution.

In order to develop an appropriate model for such a device, the selectivity of transfer across the hydrogel and nanofiber walls of these devices must be investigated. The Type 1 Diabetes device must accurately monitor glucose levels, and in turn release an appropriate amount of insulin. The research conducted analyzes the effects of variation in parameter design for such devices, while focusing on the relationship between oxygen/glucose availability and insulin production. Further, COMSOL Multiphysics® was implemented in order to optimize parameters for modeling a device via analysis of the sensitivity of insulin production to such design parameters.

2.3 Design Objectives

This study will contribute to the body of knowledge concerned with the application of cell encapsulation to Type 1 Diabetes management in the following ways:

1. Understand the modularity of insulin production by glucose and oxygen availabilities.
2. Determine the impact of incorporating multiaxial chemical species transfer capabilities on insulin production and oxygen availability.
3. Optimize the device parameters such as nanofiber thickness, hydrogel makeup (diffusivity), and islet cell loading in order to maximize insulin flux.
4. Further understand the loading of islet clusters into the device to ensure necessary aeration and maximum production of insulin for all of the cells.

Shown below in Figure 1 is a simplified schematic of the interactions between oxygen, glucose, and insulin across a cross-sectional view of a model cell encapsulation device. The design objectives address the efficiencies of these reactions as they pertain to the device.

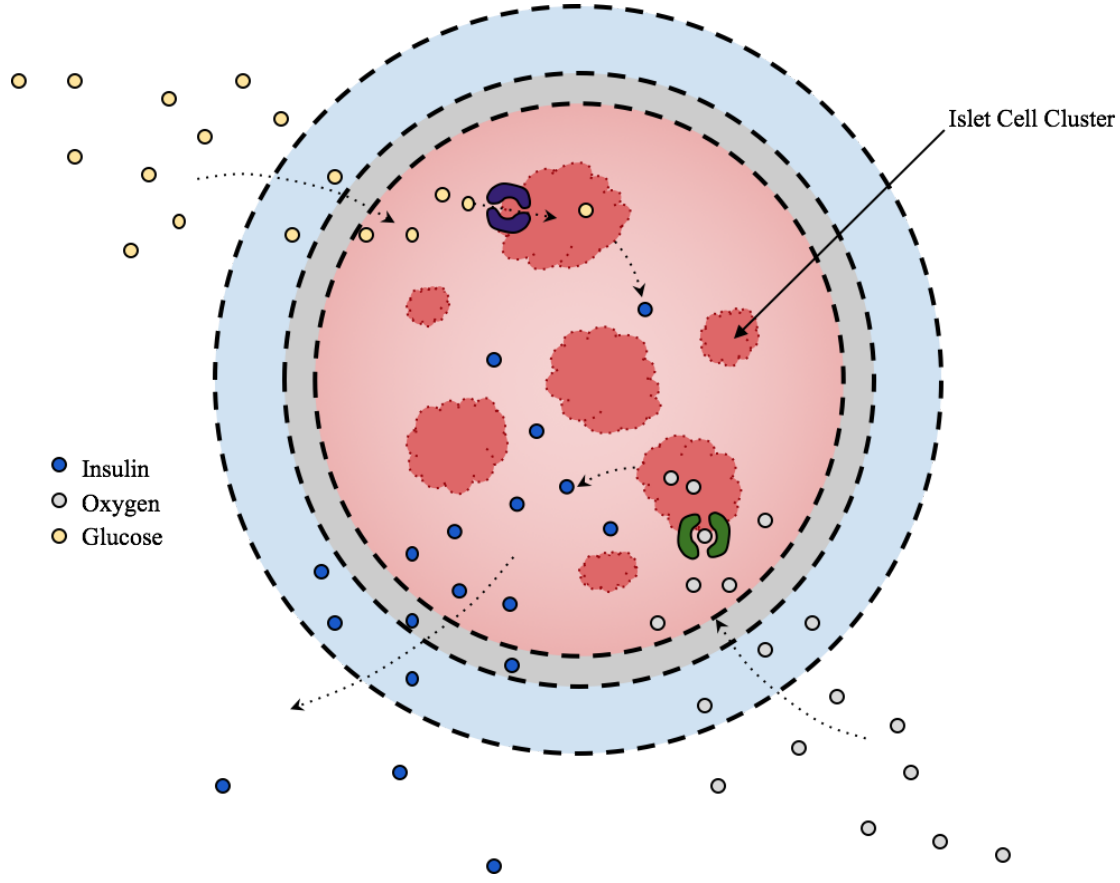

Figure 2.3.1: *Simplified schematic of device cross section.* Reveals process dynamics with focus on chemical species reactions of insulin, glucose, and oxygen. Glucose and oxygen undergo removal reactions, while insulin undergoes production reaction.

3. Schematic

3.1 Model In Vivo

The proposed means of integration for in vivo applications is to implant the device within a patient's peritoneal cavity [8]. The peritoneum is a site typically chosen for the implementation of such treatments.

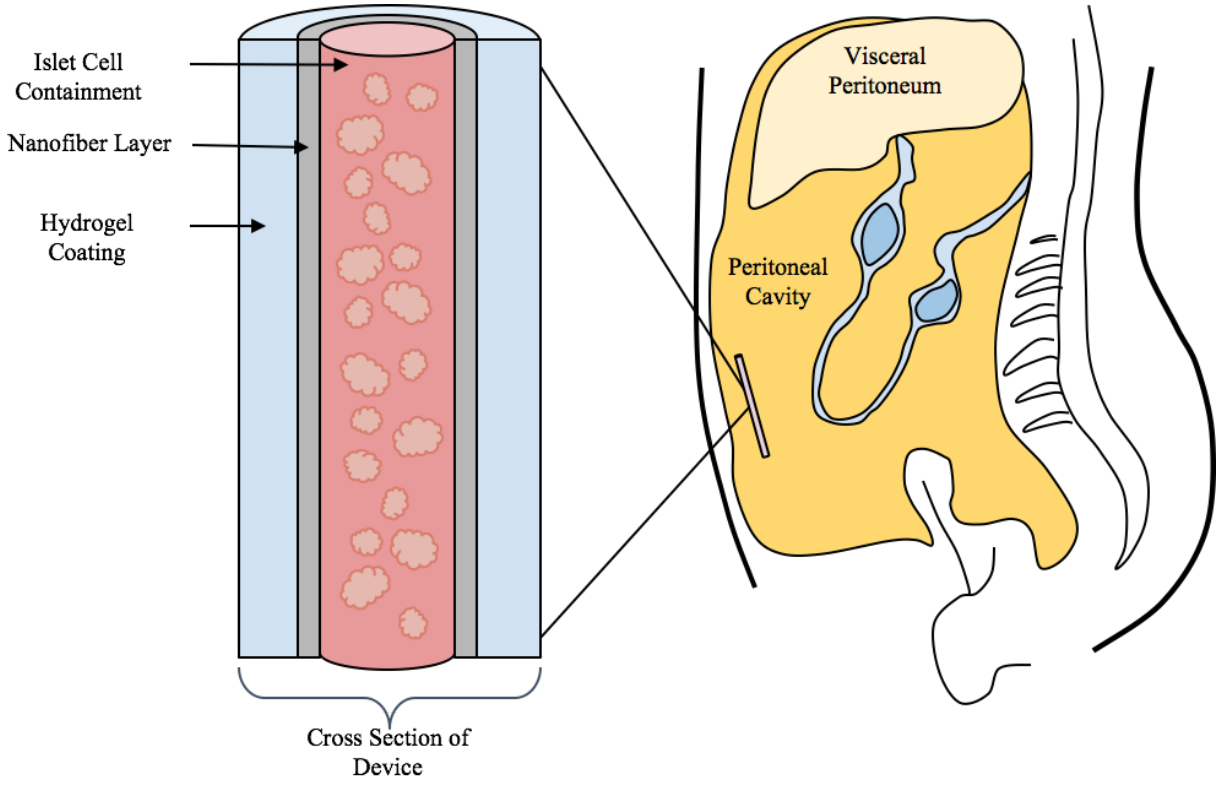

Figure 3.1.1: *Simplified schematic of device in Vivo.* Proposed design involves implantation into peritoneal cavity where device able to sense blood glucose levels and release insulin to be circulated throughout the blood and eventually to tissues.

The *in vivo* schematic was broken down into three separate models for computational analysis. Additionally this was performed in order to observe the diffusivity-driven mass transfer of chemical species, and their associated reactions. Two models, labeled No-Top Diffusion and Top Diffusion, with two-dimensional axisymmetric diffusion through both the sides of the device were implemented, the latter incorporating transport of species through the ends of the device. Many encapsulation devices feature tips which are plugged or folded, prohibiting chemical species from traveling [10]. The intention behind the implementation of these separate models was to consider the impact of incorporating ends through which chemical species may travel on oxygen availability within the device. Additionally, a two-dimensional model was developed in which islet cells were incorporated within the device as cell clusters, more closely representing the actual physiological design (Cluster Model) [10]. These models were separately implemented in COMSOL Multiphysics®. The geometry and boundary conditions of the Top-Diffusion,

No-Top Diffusion, and Cluster models are shown below in figures 3, 4, and 5, respectively. Further, throughout this paper, the Top Diffusion, No-Top Diffusion, and Cluster models are referred to as Models A, B, and C respectively.

Table 1: *Schematic-Model Chart*

Schematic	Model
No-Top Diffusion	A
Top Diffusion	B
Cluster Model	C

3.2 No-Top Diffusion Schematic - A

In order to allow for the analysis of cell encapsulation devices featuring plugged ends through which the flux of chemical species is zero, a separate model without the hydrogel and nanofiber covered ends was developed. As seen below in Figure 3, the diffusion-driven travel of the species is limited to the radial direction.

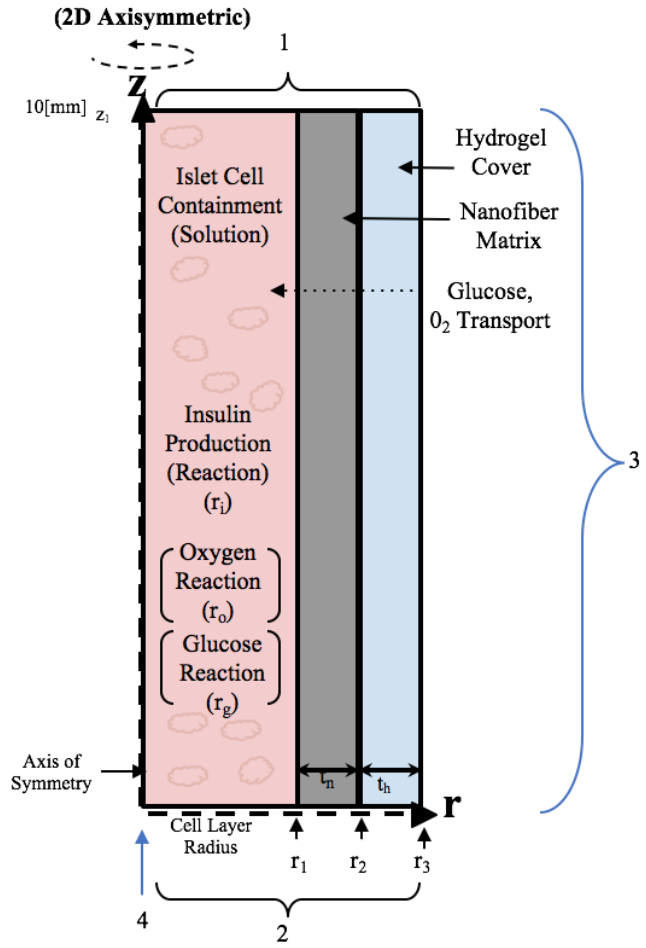

1.

$$\frac{\partial c_i}{\partial z}\Big|_{z=z_1} = 0$$
$$\frac{\partial c_g}{\partial z}\Big|_{z=z_1} = 0$$
$$\frac{\partial c_o}{\partial z}\Big|_{z=z_1} = 0$$

2.

$$\frac{\partial c_i}{\partial z}\Big|_{z=0} = 0$$
$$\frac{\partial c_g}{\partial z}\Big|_{z=0} = 0$$
$$\frac{\partial c_o}{\partial z}\Big|_{z=0} = 0$$

3.

$$C_i|_{r=r_3} = 0$$
$$C_g|_{r=r_3} = C_{Gh}$$
$$C_o|_{r=r_3} = C_{Oh}$$

4.

$$\frac{\partial c_i}{\partial r}\Big|_{r=0} = 0$$
$$\frac{\partial c_g}{\partial r}\Big|_{r=0} = 0$$
$$\frac{\partial c_O}{\partial r}\Big|_{r=0} = 0$$

Figure 3.2.1: *Model A.* The 2D axisymmetric computational model used to study the No-Top Diffusion incorporates only the radial travel of chemical species. The lines with dashes reveal the axial and radial lines of symmetry. Notice the schematic is identical to that of the Top-Diffusion model (B), save flux through the device ends. Please refer to Table 4 in the appendix to find values for parameters and variables used here [7,11-15].

Similarly to the Top Diffusion model, the No-Top Diffusion model accounts for travel in the radial direction of oxygen, insulin, and glucose. However, the 2D axisymmetric computational model representing the No-Top Diffusion device does not account for chemical species travel in the z direction as the flux of all species at the ends is considered to be zero $\text{mol} \cdot \text{m}^{-2}\text{s}^{-1}$. The decision to include a model without movement through the ends of the device had to do with the need to account for the impacts of this difference on chemical species availability. Further, the associated effects of the availability or lack of chemical species within the reactions occurring in the containment solution must be noted.

3.3 Top Diffusion Schematic - B

The schematic of the computational model featuring diffusion through both the sides of the device, and the two ends of the device is shown below in Figure 3.3.1. The geometry, boundary conditions, domains, and dimensions of this model are shown.

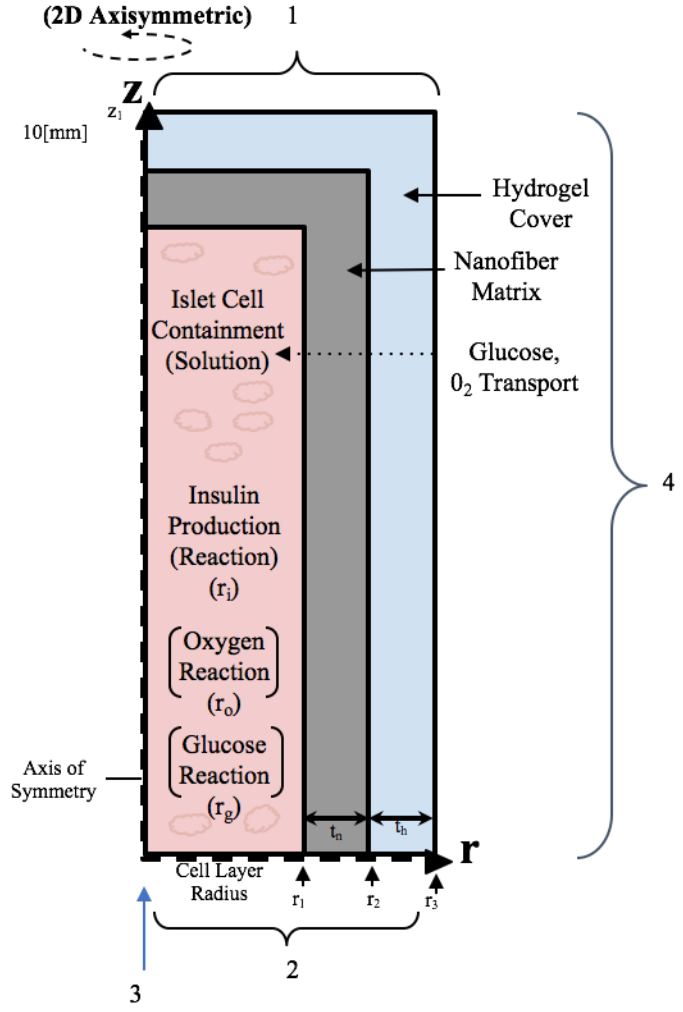

1.

$$C_i|_{z=z_1} = 0$$
$$C_g|_{z=z_1} = C_{Gh}$$
$$C_o|_{z=z_1} = C_{Oh}$$

2.

$$\frac{\partial c_i}{\partial z}|_{z=0} = 0$$
$$\frac{\partial c_g}{\partial z}|_{z=0} = 0$$
$$\frac{\partial c_o}{\partial z}|_{z=0} = 0$$

3.

$$\frac{\partial c_i}{\partial r}|_{r=0} = 0$$
$$\frac{\partial c_g}{\partial r}|_{r=0} = 0$$
$$\frac{\partial c_O}{\partial r}|_{r=0} = 0$$

4.

$$C_i|_{r=r_3} = 0$$
$$C_g|_{r=r_3} = C_{Gh}$$
$$C_o|_{r=r_3} = C_{Oh}$$

Figure 3.3.1: *Model B.* The 2D axisymmetric computational model used to study the Top-Diffusion Model incorporates both travel in the z direction, and the radial travel of chemical species. The lines with dashes reveal the axial and radial lines of symmetry. Please refer to Table 4 in the appendix to find values for parameters and variables used here [7,11-15].

The innermost domain of the 2D axisymmetric model represents the uniform containment of the islet cells. These cells have been incorporated here as a fraction of the overall solution within this containment area consisting of gel to suspend them. In the steady-state study implemented, the oxygen and glucose are incorporated as concentration values at the outermost boundaries, and travel via diffusive forces to the islet cell containment core where insulin production occurs. There is zero flux at the left boundary (z-axis) and the radial axis, reflecting the symmetric nature of the model.

3.4 Cluster Schematic - C

A third computation model was developed and implemented. As seen below in Figure 3.4.1, the 3D Cluster Model features islet cells incorporated into clusters suspended in a gel, rather than as a fraction of total containment volume.

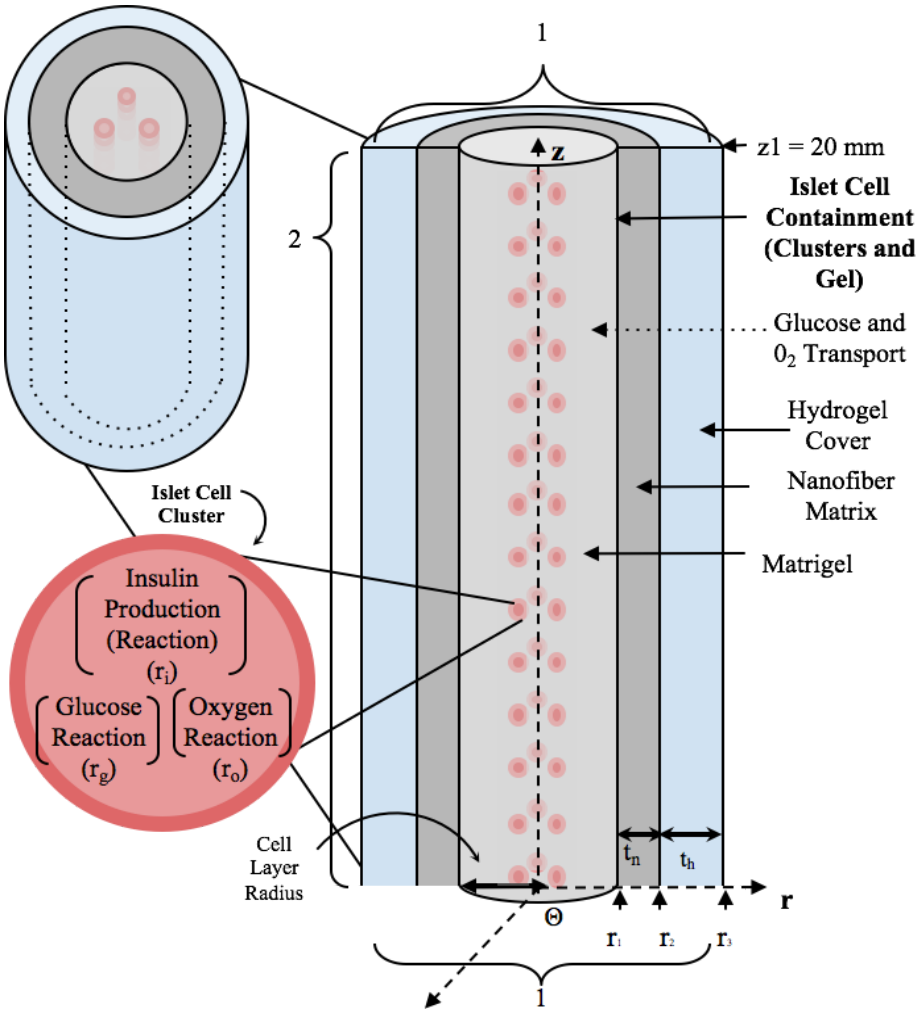

1.

$\nabla C_i = 0$

$\nabla C_g = 0$

$\nabla C_o = 0$

2.

$C_i = 0$

$C_g = C_{Gh}$

$C_o = C_{Oh}$

Figure 3.4.1: *Model C*. The 3D computational model used to study the Cluster Model incorporates islet cells as clusters. Notice the schematic is similar to that of the No-Top-Diffusion model (schematic A), save representation of the islet cells as a volume percentage of the containment and rather as clusters. The lines with dashes reveal the axial and radial lines of symmetry. Please refer to Table 4 in the appendix to find values for parameters and variables used here.

The Cluster Model incorporates the islet cell component of the device into cell clusters suspended in a gel solution. Rather than considering such cells as a percentage of total volume within the cell containment (a feature implemented in other models for computational simplicity), the Cluster Model more closely represents the reality of islet cell loading in cell encapsulation devices. The cluster sizes were exaggerated in this model by a factor of 8 in order to compare the impacts of incorporating the minimum islet cell sizing (a percentage of a uniform solution), and a much larger cell parameter sizing (in the form of clusters) on the use of oxygen and the secretion of insulin within the device.

4. Methods

4.1 Governing Equations - Models A, B

The physics models implemented primarily involve mass transfer of three separate chemical species—oxygen, glucose, and insulin—as well as reactions occurring amongst and between these species. The steady-state model accounts for the travel of oxygen and glucose through the device from the outermost walls via the implementation of concentration boundary conditions and necessary diffusion terms in each of the three primary domains. Since there are three different layers within the model—a nanofiber matrix layer, hydrogel layer, and an inner islet cell containment layer—a single governing equation has been implemented across the three domains, with the reaction term for each chemical species in these regions changing as specified below. The values for parameters and variables used here may be found in Table 4 in the appendix. The addition of chemical species movement in the z direction for the Model B implemented required a separate governing equation (Equation 2) to be used to account for this new direction of mass transfer not present in the No-Top Diffusion model (Equation 1).

The percentage of islet cells within the uniform containment solution are accounted for mathematically within the equations through multiplying the Michaelis Menten reactions by the islet load (z) which has been inputted as a percentage. The non-zero reaction terms within the islet containment core are each executed in the computational analysis with the addition of a smooth heavy side function to the Michaelis Menten Kinetics used. The heavy side function returns a value of zero for the cases in which oxygen concentration drops below critical oxygen value that indicates cell death has occured and reactions no longer take place [14].

A - No-Top Diffusion: $$D_j[\frac{1}{r}\frac{\partial}{\partial r}(r\frac{\partial c_j}{\partial r})] + r_j = 0 \quad (1)$$

B - Top-Diffusion: $$D_j[\frac{1}{r}\frac{\partial}{\partial r}(r\frac{\partial c_j}{\partial r}) + (\frac{\partial^2 c_j}{\partial z^2})] + r_j = 0 \quad (2)$$

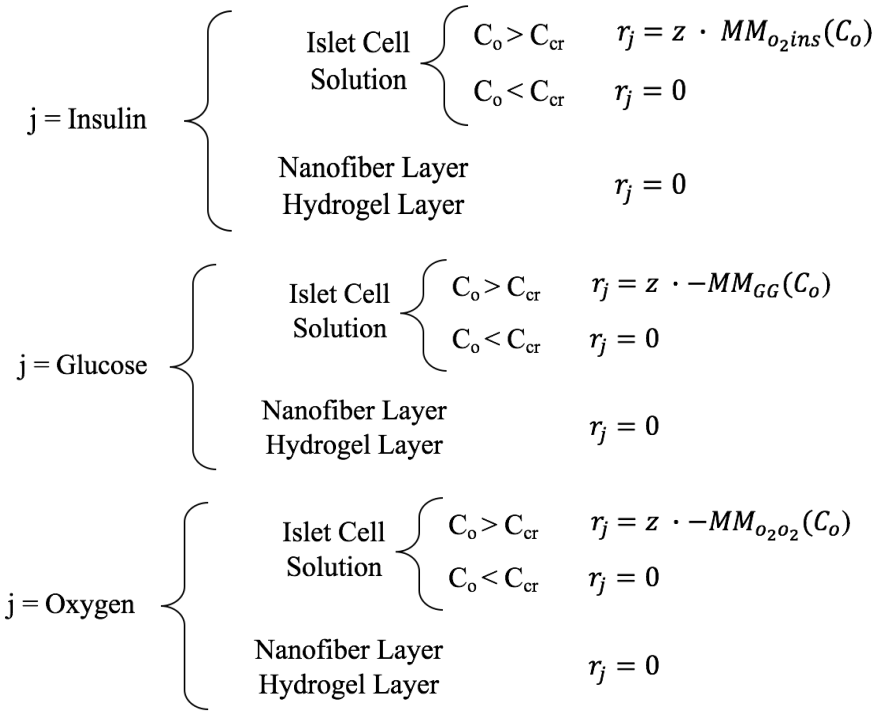

Table 2: *Diffusivity Value Chart - A,B*

Diffusivity	Islet Core	Nanofiber Layer	Hydrogel (alginate)
D_i	$D_{i\ ECM}$	D_{in}	$D_{i\ Alg}$
D_g	$D_{G\ ECM}$	$D_{G\ N}$	$D_{G\ Alg}$
D_o	D_{O2ECM}	D_{O2N}	D_{O2Alg}

4.2 Governing Equations - Model C

The physics model implemented in Model C includes hydrogel and nanofiber layers represented equivalently in Model A, yet a different islet cell implementation which involves an additional domain absent from the models mentioned earlier. As the islet cells are no longer represented by a percentage concentration in a uniform gel solution, but rather as clusters suspended within a gel, the cells and the gel are separated in the model to create two different domains within the islet containment core. In the previous model, the islet cell amount in the containment was accounted for by multiplying Michaelis Menten reactions by an islet load. Here, the Michaelis Menten reactions are no longer abated by islet load percentages as before, and are instead restricted to occurring within each of the clusters. Additionally, this fourth domain belonging to the matrigel is accompanied by the need for another equation as is discussed below (Equation 3). Because the addition of individual clusters removes an axisymmetric assumption, a 3D model became necessary.

$$\text{C - } \textit{Clusters}: \quad D_j\left[\frac{1}{r}\frac{\partial}{\partial r}\left(r\frac{\partial c_j}{\partial r}\right) + \frac{1}{r^2}\left(\frac{\partial^2 c_j}{\partial \theta^2}\right) + \left(\frac{\partial^2 c_j}{\partial z^2}\right)\right] + r_j = 0 \qquad (3)$$

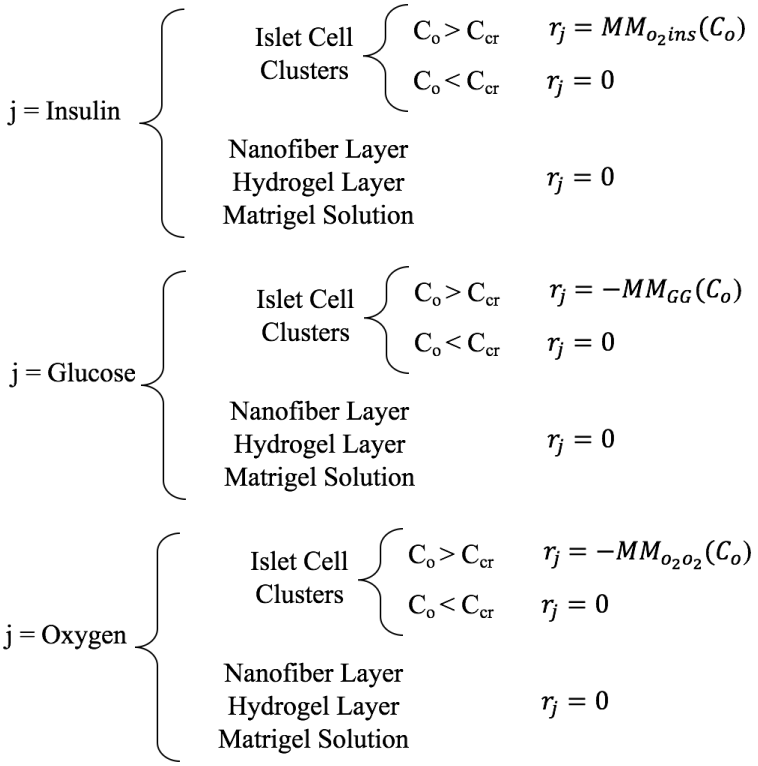

Table 3: *Diffusivity Value Chart - C*

Diffusivity	Islet Core, Matrigel	Nanofiber Layer	Hydrogel (alginate)
D_i	$D_{i\ ECM}$	D_{in}	$D_{i\ Alg}$
D_g	$D_{G\ ECM}$	$D_{G\ N}$	$D_{G\ Alg}$
D_o	D_{O2ECM}	D_{O2N}	D_{O2Alg}

4.3 Boundary Conditions

Table 1: Summary of Boundary Conditions Implemented in Models A and B

Schematic	Insulin	Glucose	Oxygen
A	$\frac{\partial c_i}{\partial r}\|_{r=0} = 0$ $C_i\|_{r=r_3} = 0$ $\frac{\partial c_i}{\partial z}\|_{z=z_1} = 0$ $\frac{\partial c_i}{\partial z}\|_{z=0} = 0$	$\frac{\partial c_g}{\partial r}\|_{r=0} = 0$ $C_g\|_{r=r_3} = C_{Gh}$ $\frac{\partial c_g}{\partial z}\|_{z=z_1} = 0$ $\frac{\partial c_g}{\partial z}\|_{z=0} = 0$	$\frac{\partial c_O}{\partial r}\|_{r=0} = 0$ $C_o\|_{r=r_3} = C_{Oh}$ $\frac{\partial c_o}{\partial z}\|_{z=z_1} = 0$ $\frac{\partial c_o}{\partial z}\|_{z=0} = 0$

B	$\frac{\partial c_i}{\partial r}\|_{r=0} = 0$ $C_i\|_{r=r_3} = 0$ $\frac{\partial c_i}{\partial z}\|_{z=0} = 0$ $C_i\|_{z=z_1} = 0$	$\frac{\partial c_g}{\partial r}\|_{r=0} = 0$ $C_g\|_{r=r_3} = C_{Gh}$ $\frac{\partial c_g}{\partial z}\|_{z=0} = 0$ $C_g\|_{z=z_1} = C_{Gh}$	$\frac{\partial c_O}{\partial r}\|_{r=0} = 0$ $C_o\|_{r=r_3} = C_{Oh}$ $\frac{\partial c_o}{\partial z}\|_{z=0} = 0$ $C_o\|_{z=z_1} = C_{Oh}$

4.4 Assumptions

The following assumptions have been made in order to develop the computational models, as well as their accompanying governing equations and boundary conditions. These assumptions were created based on information gathered from literature, as well as through consultation with laboratories pursuing applicable research.

- No additional adsorption occurs within the nanofiber mesh or the hydrogel, as these regions are already saturated with chemical species.
- Insulin activity at the outermost boundary can be accounted for through implementing a concentration boundary condition of zero mol m^{-3}, reflecting total removal and consumption of the insulin by the surroundings.
- No hydrophobic effects impact the travel of chemical species across the device.
- Assume peritoneum is well mixed [7]
- Insulin is secreted from cells in form of monomers alone, while dimers and hexamers are not secreted. Chemical equilibrium is driven toward monomers as a result of Le Chatelier's principle.
- The nylon mesh layer is completely impregnated by the hydrogel.
- Fibrosis, the process through which the immune system creates an impenetrable fibroblast barrier around foreign objects, is negligible [8]. Therefore, the diffusion of chemical species is not affected by cellular activity around the device (other than insulin consumption).
- The hydrodynamic radius of insulin may be used as an accurate value for the purposes of these models [16]. This can then be used in conjunction with an appropriate obstruction model in order to determine the diffusivity of insulin in the nylon layer, the calculations of which may be found in the appendix [17].
- Islet load does not affect confinement diffusivity significantly.

5. Results and Discussion

In developing plots and figures to display the results obtained from the study, a standard device model was chosen and maintained throughout all the figures save when mentioned otherwise, or in the cases where parameter changes were performed. This standard model was the model B, and featured an islet load of .005, nanofiber (nylon) layer of 100 microns, and alginate as the hydrogel component. The models with which each of the figures are concerned are listed in parentheses following the figure number.

5.1 Glucose Modulation

Prior research suggests glucose to be the essential modulator of insulin production for cell encapsulation devices [17]. To further determine the effects of glucose on the steady state secretion of insulin following a meal, insulin concentration was modelled at two blood glucose concentrations both of which reflected after a meal. Figure 5.1.1 below illustrates that insulin secretion varies minutely with the glucose concentration immediately outside of the device, which you can particularly note by only the slight change in insulin concentration.

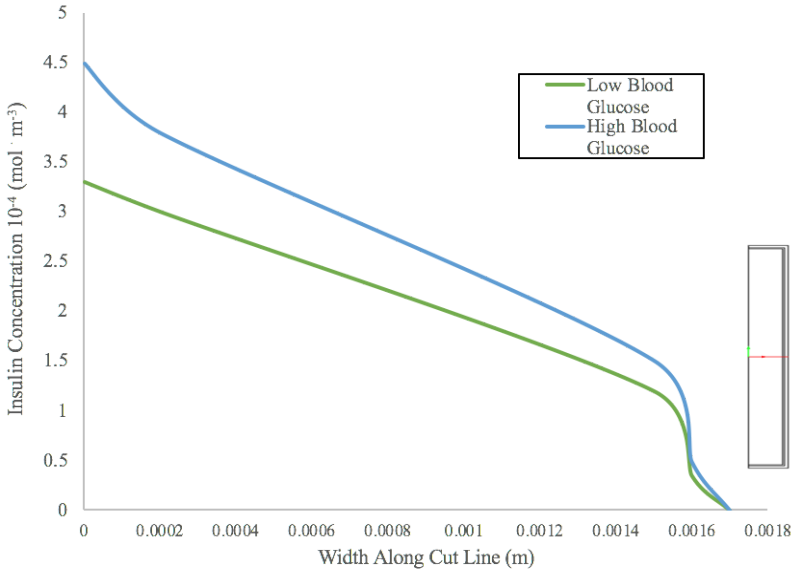

Figure 5.1.1 (B): *Modulation of insulin concentration by glucose during steady-state following a meal*. Low blood glucose corresponds to a value of 5.56 mol·m^{-3} and high blood glucose values correspond to 11 mol·m^{-3} [10].

Within regular conditions, glucose is an important modulator of insulin secretion and is the basis for why this device can be used for long term treatment of diabetes. However, the model follows steady state conditions following a meal in order to optimize the device to account for when maximal insulin is being produced and secreted. Therefore, glucose acting as a modulator was assumed to be insignificant for the rest of this report. This lack of change in insulin levels throughout the device is accompanied by an equivalent lack of change in glucose concentration across the device, as shown below in Figure 5.1.2.

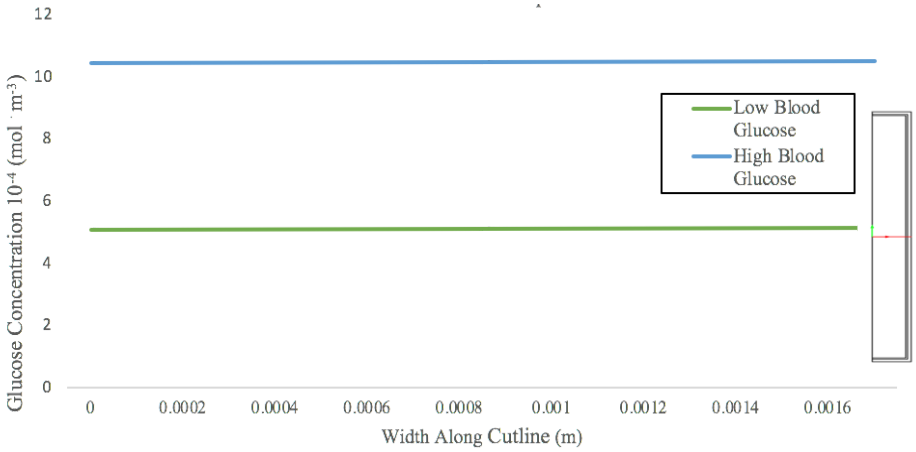

Figure 5.1.2 (B): *Glucose concentration throughout device changing radially.* This figure shows relatively constant glucose concentration throughout the device and little insulin production modularity, as this model reflects the device immediately after the user has consumed food.

The process reflected here shows that for steady state concentration, the glucose levels are relatively constant throughout the device and do not play as large a role as other reagents in the secretion of insulin. For additional figures of chemical species in these devices, please refer the contour plots in Appendix E.

5.2 Oxygen Availability

After determining that glucose was not the primary modulator, oxygen availability to the islets was considered next. Oxygen is the other important modulator of insulin secretion and plays an important role in keeping the islet cells alive. At low concentrations of oxygen, islets furthest from the outermost radius of the device will begin to die (necrosis occurs). Therefore, the device geometry was altered and the maximal radii of the core was set to a width such that islets within the center of the device still receive the minimum concentration of oxygen necessary to stay alive. In other words, the effective concentration of oxygen was the actual subtracted by the critical oxygen required (Equation 9 in appendix). Figures 5.2.1 and 5.2.2 show different maximal widths given changes of hydrogel composition or nanofiber matrix layer.

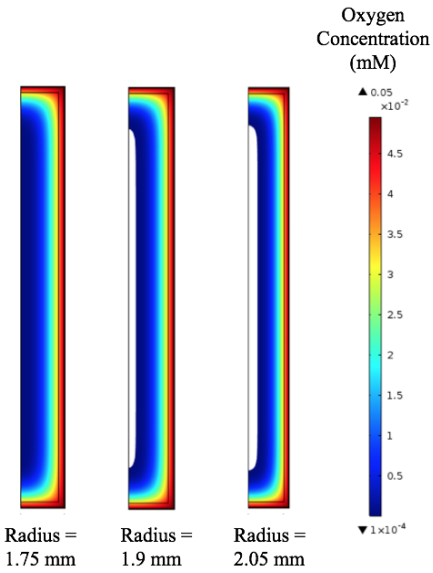

Figure 5.2.1 (B): *COMSOL generated surface plots of critical radii.* Reveals cell death when Islet Containment Radius goes over maximum.The death of islet cells is due to a lack of oxygen to sustain life. This was calculated by subtracting critical oxygen concentration from the oxygen concentration at a particular location along the r/z-axes.

If the radii of the device exceeds the maximal width, as shown in Figure 5.2.1 islets will begin to succumb to hypoxia and die, as shown by the white portions of this figure. Thus, critical radii is a key parameter that a research team would have to test for to determine the optimal parameters such that all islet cells are able to live all throughout the device. Applying this method to next find the optimal nylon nanofiber matrix thickness to also promote optimal oxygen transport into the device to keep the cells alive, as you will note in the next Figure 5.2.3.

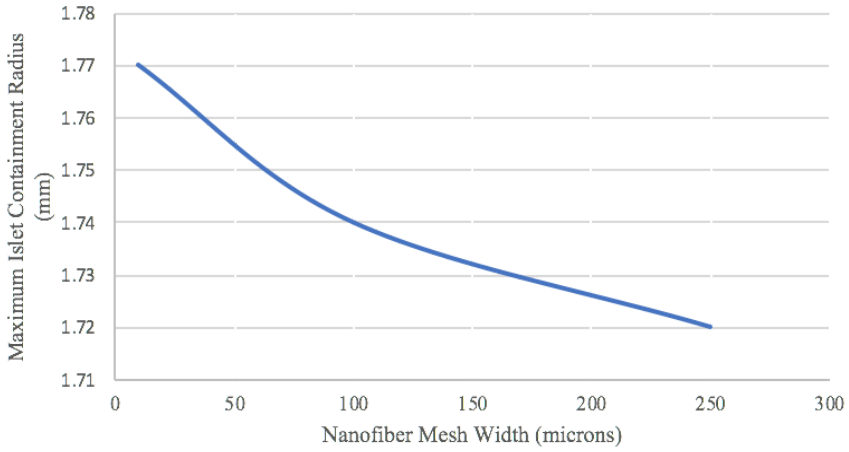

Figure 5.2.3 (B): *Maximum Islet Containment Radius in relation to Nanofiber Matrix.* Analyzed via oxygen availability across the radii of the nanofiber mesh. Analyzed via cell death within the device due to restraints in oxygen availability.

This data illustrates that the thinner than nylon nanofiber matrix width is, the higher the oxygen transport is across the membrane. This aids in determining an optimal thickness of Nylon that both enables the device to be sturdy as well as enhances/lengthens life of islet cells. Determining the critical radii and the effects of going beyond the maximum width of the islet cell containment solution was analyzed further in different types of islet cell solutions.

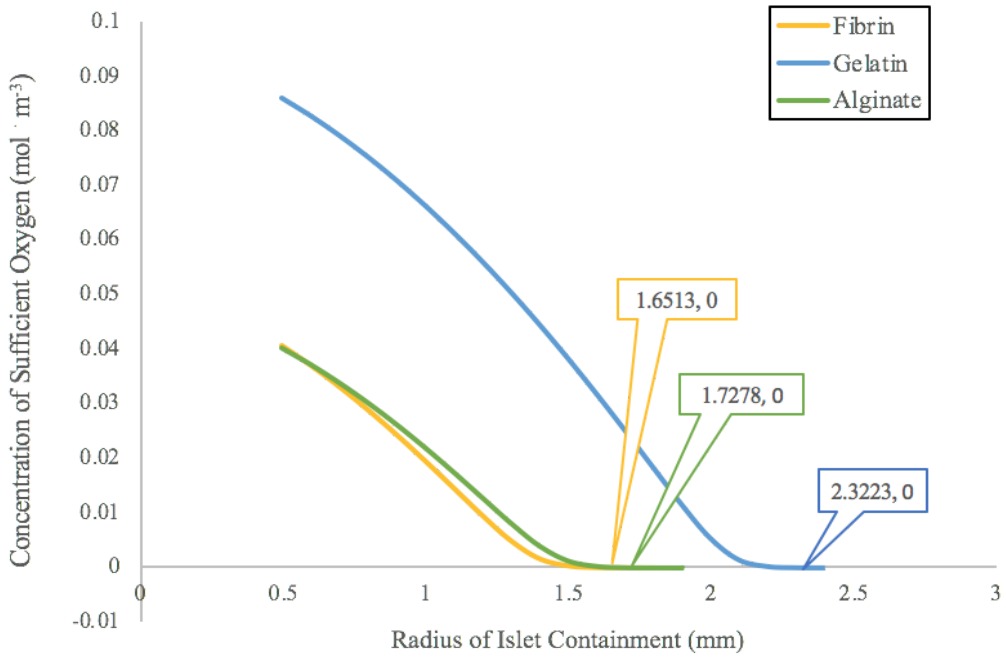

Figure 5.2.3 (B): *Critical Islet Containment Solution Radius for different types of hydrogels.* Fibrin, Gelatin, and Alginate were analyzed due to their biocompatibility and desirable diffusivities for oxygen, insulin, and glucose transport.

Figure 5.2.3 illustrates how gelatin would be considered the most optimal option, as gelatin has the largest critical radius, allowing for the device to support more islet cells in providing more oxygen.

Since oxygen is the primary modulator of this cellular encapsulation device, using varying oxygen levels to determine which thickness of nylon is most beneficial as well as type of hydrogel to recommend using is essential. Of the three types of hydrogel implemented, gelatin has the highest solubility constant for oxygen, and therefore the maximal width of the device is 2.26 millimeters as compared to the maximal width of 1.74 millimeters and 1.62 millimeters for alginate and fibrin, respectively [11, 15, 20]. Even though gelatin has smaller diffusion coefficients for the chemical species of importance for this device, it still secretes a larger amount of insulin as compared to devices composed of alginate or fibrin, as shown in Figure 5.4.10 [18, 21-22]

5.3 Multiaxial Diffusion

In developing these devices, there is variation with regards to whether or not diffusion through the ends of cell encapsulation devices is accounted for or incorporated. Often, the ends of these devices are plugged or sealed off with thermo-sealers in order to prevent leakage of the device's islet cell containment [10]. Shown below in Figure 5.3.1 is a comparison of the overall insulin flux of model B, in which diffusion through both the radial and z-axis directions is allowed, to that of model A which only allows radial chemical species transfer.

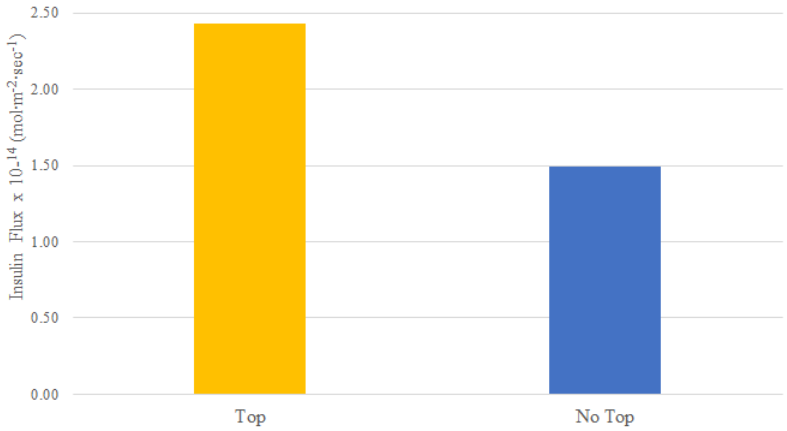

Figure 5.3.1 (B, A): *Insulin Flux in Top Diffusion and No-Top Diffusion.* The derived insulin fluxes through the Top and No-Top Diffusion models (B,A) are shown here, as the insulin flux for B here represents the sum of the flux out in the radial direction and the flux out in the z-axis direction.

The calculated flux of insulin out of the hydrogel layer of the devices differ significantly between models A and B. The total insulin flux for the model with transfer in more than one direction was $2.43 \cdot 10^{-14}(\text{mol} \cdot \text{m}^{-2}\text{s}^{-1})$, while the other model which featured transfer only in the radial direction was determined to have a flux value of $1.49 \cdot 10^{-14}(\text{mol} \cdot \text{m}^{-2}\text{s}^{-1})$. This comparison reflects the larger insulin flux that is associated with allowing movement of chemical species to be multidirectional. In addition to considering the impact of incorporating this multidirectional transfer on insulin flux, the radius of Islet Confinement was chosen as another parameter of significance to study for variation between the two models as shown in Figure 5.3.2 below.

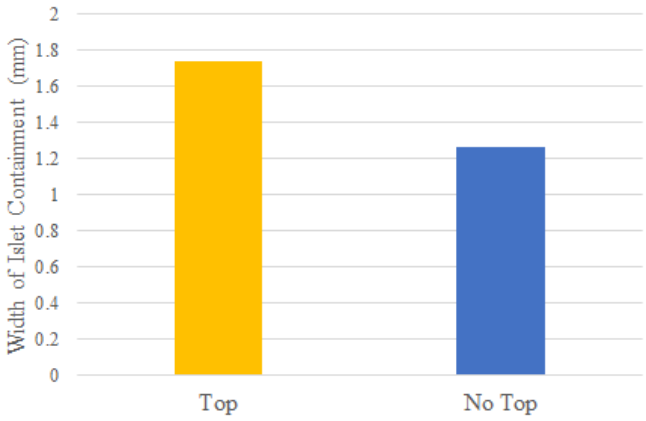

Figure 5.3.2 (B, A): *Critical Containment Radius in Top Diffusion and No-Top Diffusion.* In subtracting the critical oxygen concentration (ccr) from total oxygen concentration, these critical radii of the Islet Containment aspect of the two different models were calculated.

The incorporation of multiaxial transfer allowed for B to have a larger critical radius, and thus contain higher concentration of oxygen in the interior. At a value of 1.75 mm, the radius of B was evaluated to be larger than the critical radius of A, evaluated to be 1.26 mm. Both models were implemented in the COMSOL study using the critical radius value of model A (1.75 mm) in order to visualize and compare levels of cell death between the devices, as indicated by the white region shown in the surface plots below in Figure 5.3.3.

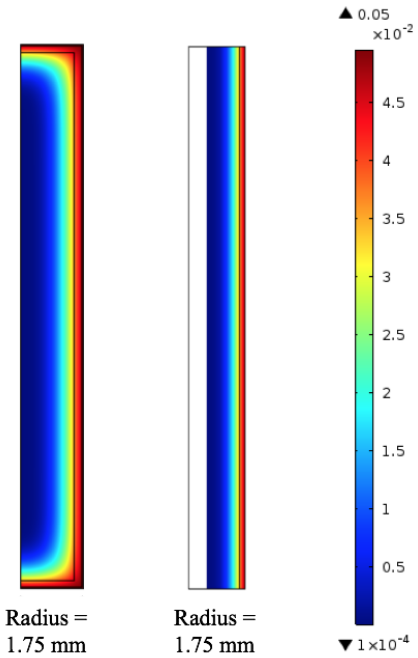

Figure 5.3.3 (B): *COMSOL generated surface plot of A and B modeled necrosis*. Both modeled with a islet confinement radius of 1.75 mm. Necrosis is revealed by the white regions of the plots, as the critical oxygen value is reached.

These studies served to quantify the disparities between A and B with regards to insulin flux and critical radius values and associated amounts of necrosis. In incorporating multiaxial chemical species transfer, both the insulin production and the availability of oxygen were strongly impacted. As seen in Figures 5.3.1 and 5.3,2, models A and B were used to show that oxygen availability and insulin production increase with the implementation of multiaxial transfer, as is revealed by the critical confinement radii and the insulin fluxes. These studies on the impact of multiaxial transfer were considered in identifying B (Top-Diffusion) as an optimal model on which later studies and problems pertaining to insulin flux were conducted. However, as the length of these devices increase, the difference between the insulin fluxes for the two models is expected to decrease.

5.4 Insulin Flux

As the studies on oxygen availability revealed its high modulatory impacts on insulin production, specific parameters of the device were assessed in the process of optimization to further understand additional effects of these parameters on insulin production. Three of the highly customizable aspects of the device were chosen and studied with regards to their impact on the insulin flux specifically using the B model as a standard base model across the studies.

In order to maintain the structure of the cellular encapsulation devices, it is necessary to integrate the backbone structures that prevent the devices from collapsing and other deformities. As the nanofiber (nylon) mesh layer surrounds and confines the islet cell containment core, the impacts of variation in the mesh were studied as seen below in Figures 5.4.1 and 5.4.2 to observe insulin flux brought about by the use of large mesh layers across two different cut lines.

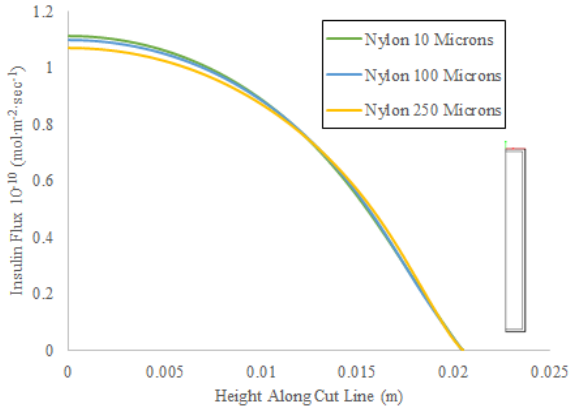

Figure 5.4.1 (B): *Insulin flux along upper cut line at various nylon layer thicknesses.* Three thicknesses were implemented and the insulin flux along cut line was calculated.

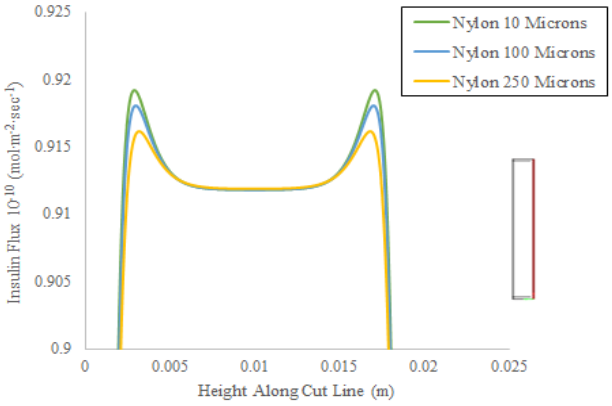

Figure 5.4.2 (B): *Insulin flux along height cut line at various nylon layer thicknesses.* Three thicknesses were implemented and the insulin flux along cut line was calculated.

In the implementation of three different nylon layer thicknesses of 10, 100, and 250 microns, insulin flux was analyzed at the two cut lines and only varied a little with regards to the nylon thicknesses. A more comprehensive understanding of these results may be attained through the study of Figure 5.4.3 below, which reveals the impact of increasing the width of the nylon mesh layer on the flux of the insulin out of the device.

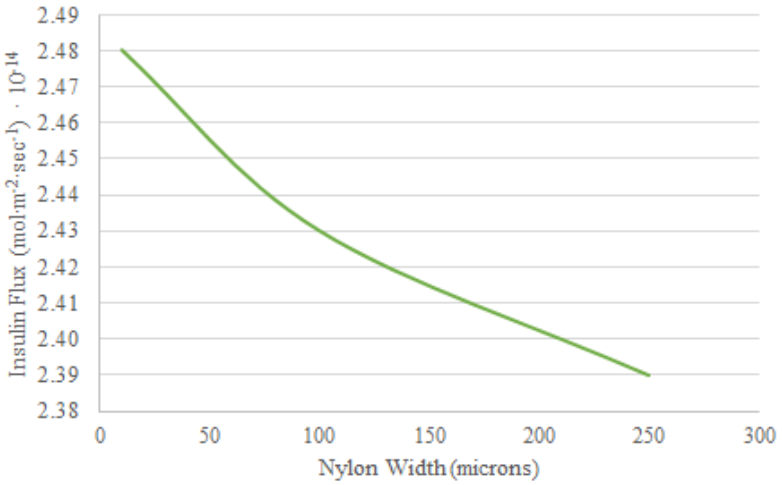

Figure 5.4.3 (B): *Insulin flux as a function of nylon width*. The width of the nylon mesh layer is increased from 10 to 250 microns, and the insulin flux is plotted for a device with variety of thicknesses.

The first parameter analyzed with regards to its impacts on the study of insulin flux was the width of the nanofiber (nylon) layer of the device. In the model, the nylon layer is modeled as a sheet impregnated with hydrogel. A decrease in pore size associated with this impregnation primarily affects larger molecules such as insulin, as the hydrodynamic radius of insulin is three orders of magnitude larger than a glucose molecule. As the hydrodynamic radius of a solute increases, the likelihood for it to diffuse through a pore path from one end of the hydrogel to the other is reduced as is reflected by a decrease in diffusion [17, eq (5)], as well as the Figures 5.4.1, 5.4.2, and 5.4.3. Minimizing the width of the nylon layer would maximize the insulin secretion from this device at steady state. The Young's modulus of nylon is over four orders of magnitude larger than alginate [23-25]. To ensure the stability and fidelity of these devices, a minimum amount of nylon must be used in order to maximize the secretion of insulin.

One of the major concerns of such a device is ensuring ease of implantation and removal, as these are paramount concerns to ensure the wellbeing of the patients being treated. As islet load increases, the maximal radius of the device decreases, thereby making the device overall smaller and easier to implant and remove. Next, Model B was remade with varying islet loads. Islet load (z) is the percentage of the core that is made up of cells. Please note in the first Figure, 5.4.4, below the trend of the graph.

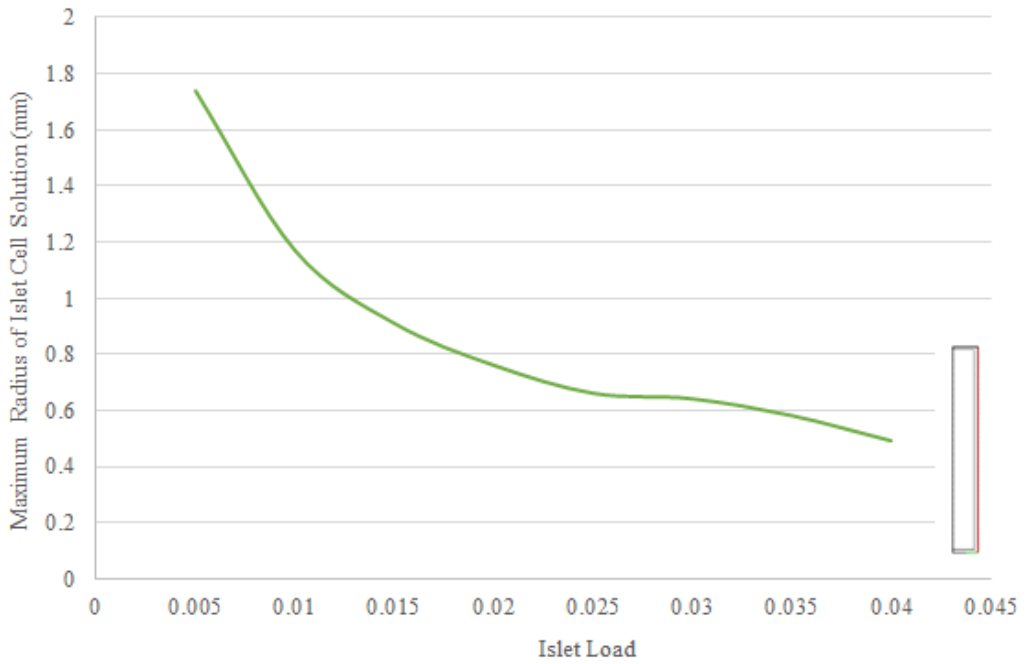

Figure 5.4.4 (B): *Variation of Islet Load's effect on the Maximum Radius of Islet Cell Solution.* Used by calculating the critical radius as a function of oxygen concentration present-critical concentration of oxygen.

However, Model B had a lower insulin secretion from the device with higher islet loads. If the islet loading is increased due to decreasing the size of the device, less insulin will be secreted as a device with the same number of cells at a lower islet load. Effectively, islet load describes the density of the cells within the core. Physiologically, as cells get closer to each other and aggregate into larger colonies, it becomes easier to create hypoxic cores within which these colonies can no longer produce insulin [7]. To analyze the effects of islet load on this device, insulin flux was next tested in Model B as seen below in Figures 5.4.5 and 5.4.6.

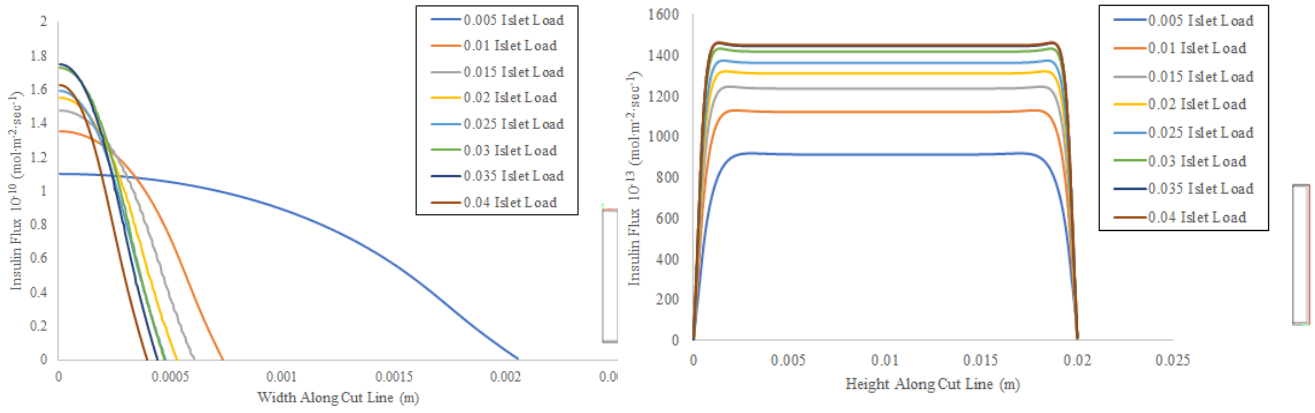

Figure 5.4.5 (B): *Insulin flux along upper cut line radially with differing islet loads*. Islet loads of 0.005, 0.01, 0.015, 0.02, 0.025, 0.03, 0.035, and 0.04 were analyzed across these layers.

Figure 5.4.6 (B): *Insulin flux along height cut line of device with differing islet loads.* Islet loads of 0.005, 0.01, 0.015, 0.02, 0.025, 0.03, 0.035, and 0.04 were analyzed across these layers.

Both of Figures 5.4.5 and 5.4.6 also illustrate that as islet load increases, total insulin flux decreases. Furthermore, both of these models were combined to solve for total insulin flux in relation to islet load as can be seen below in Figure 5.4.7.

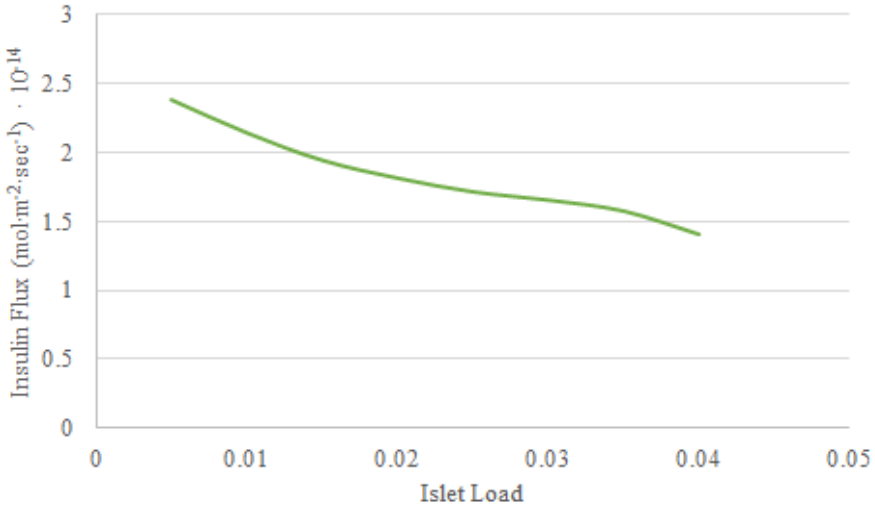

Figure 5.4.7 (B): *Total effect of total insulin flux with differing islet loads.* Mass transfer occurs radially and across z-axis. Islet loads of 0.005, 0.01, 0.015, 0.02, 0.025, 0.03, 0.035, and 0.04 were analyzed across these layers.

This final graph seen in Figure 5.4.7 further emphasizes the adverse effect that increasing islet load has on the production of insulin. While inserting a smaller device is more convenient for the patient, the effectiveness of the device will decrease.

The third parameter studied with regards to its effects on the levels of insulin flux from the device was the type of hydrogel implemented in order the create the hydrogel coating layer. The hydrogel component of the model constitutes the majority of the confinement layer. Each change in hydrogel type was also accompanied by the need for consideration of different oxygen solubilities for the hydrogels, as well as the incorporation of different diffusivities [10-15,18-21,23]. Three types of hydrogel were implemented below in Figures 5.4.8 and 5.4.9 in order to understand the insulin flux modulatory properties of the outermost device layer. Alginate, gelatin, and fibrin are commonly used in similar applications and were implemented here for this reason. The diffusivities, oxygen solubility coefficients, and other applicable terms for the different gels may be found in Table 4 in the appendix.

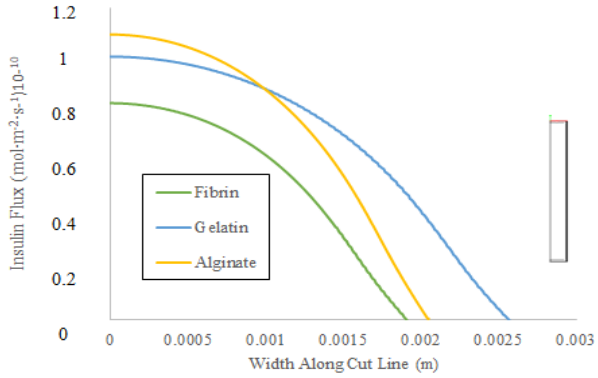

Figure 5.4.8 (B): *Insulin flux along upper cut line for different hydrogels.* Three different types of hydrogel are implemented, and the insulin flux of the B model's upper cut line with each of these hydrogels is plotted.

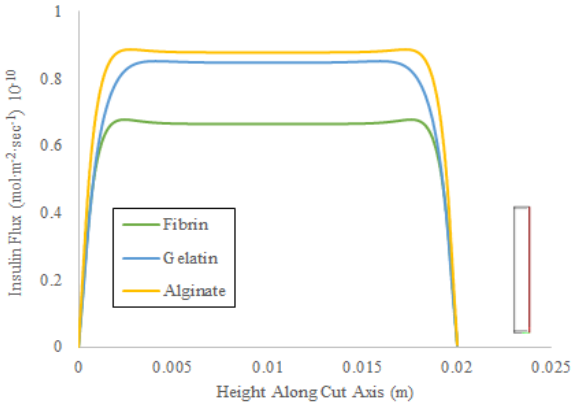

Figure 5.4.9 (B): *Insulin flux along height cut line for different hydrogels.* Three different types of hydrogel are implemented, and the insulin flux of the B model's height cut line with each of these hydrogels is plotted.

For the upper cut line, fibrin was determined to provide the lowest insulin flux of all three hydrogel types across all widths, indicating its inefficiency in acting as a hydrogel coating for these specific applications. While alginate initially exceeded the gelatin with regards to insulin flux, the insulin flux provided by the gelatin coated model surpassed the flux of alginate near the 1 mm mark along the cut line. Taking the sum of the upper cut line and the height cut line, the total insulin flux for each gel is shown below in Figure 5.4.10.

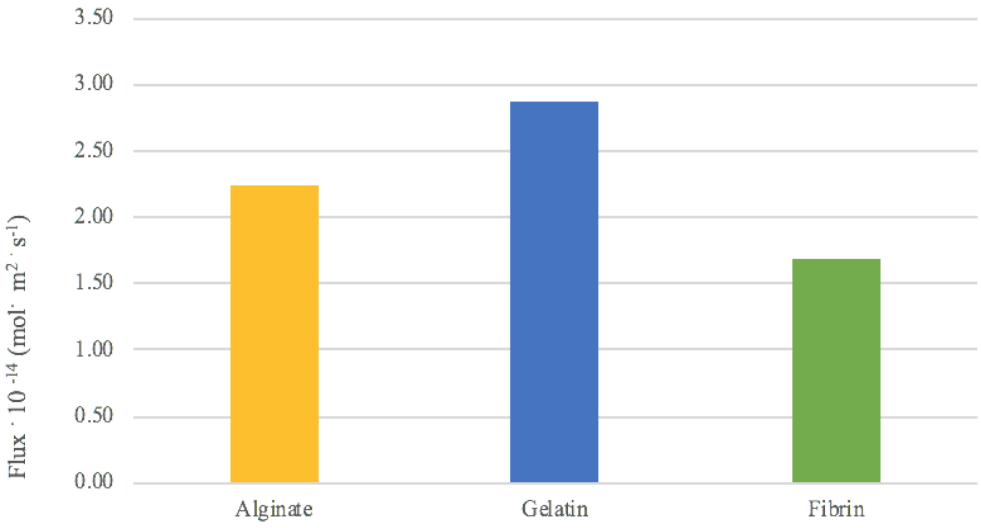

Figure 5.4.10 (B): *Total insulin flux for B model using gelatin, fibrin, and alginate.* Three different types of hydrogel are implemented, and the total insulin flux of each hydrogel model is generated through summing calculated fluxes at the upper cut line and height cut along the axis.

Two values of significance for this optimization study are the solubility of oxygen within each hydrogel, as well as the diffusivity of chemical species within each. As the solubility of oxygen in the hydrogel increases, a greater amount of the partial pressure of oxygen in the surroundings (peritoneal cavity) can diffuse into the hydrogel. As the diffusivities increase for a chemical species, diffusion across the hydrogel layer occurs more rapidly, and greater amounts of oxygen are able to propagate into the device to support a larger number of cells and critical islet confinement radius [13] .

Of the three types of hydrogel implemented in the model, the use of gelatin in developing the hydrogel coating of the Model B allowed for an insulin flux of $2.86 \cdot 10^{-14}$ ($mol \cdot m^{-2}s^{-1}$). The use of alginate was less conducive to high insulin flux for Model B, and a flux of $2.24 \cdot 10^{-14}$ ($mol \cdot m^{-2}s^{-1}$) was determined. Fibrin was consistently less conducive to optimal insulin flux, as revealed by a relatively lower flux of $1.68 \cdot 10^{-14}$ ($mol \cdot m^{-2}s^{-1}$).

5.5 Cluster Model

The three-dimensional cluster model (Model C) is a more accurate representation of this device in physiological conditions. The difference between Model C and both Models A and B is that rather than using a homogeneous partial fraction of a uniform solution to evenly disperse the beta cells in the islet cell containment solution, the cells would be grouped as clusters (shown below in Figure 5.5.1 as part of a COMSOL slice plot) randomly dispersed throughout the media.

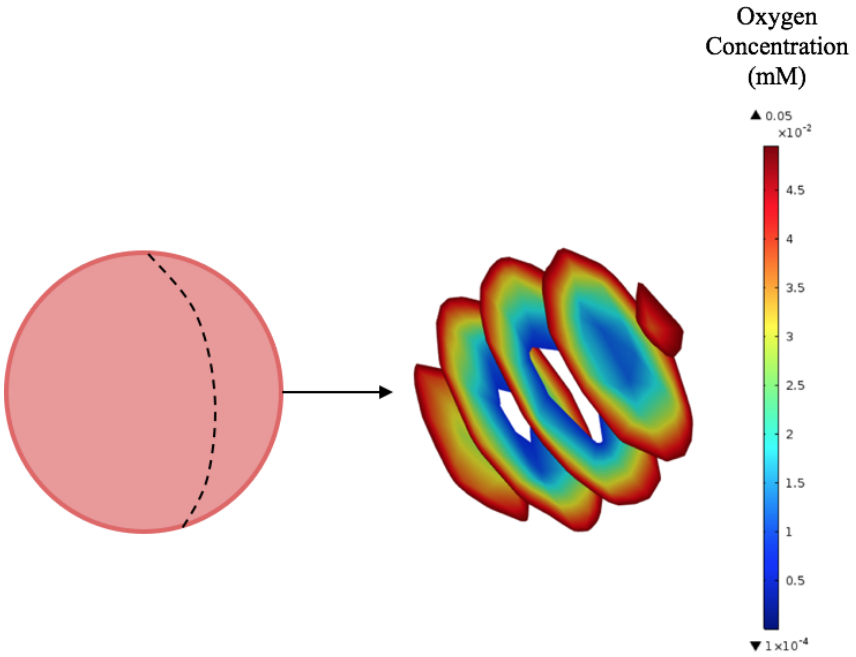

Figure 5.5.1 (C): *Diagram and COMSOL slice plot of islets in cluster*. islet cells in a cluster at steady state. The white/clear area represents the middle of the cluster where cell death has occurred.

As cells aggregate into larger clusters, the islets located closer to the central radius easily die to due lack of availability of oxygen as shown in Figure 5.5.1 [7]. The inner part of the figure represents cells that are below the necessary oxygen concentration to survive. As this model is more complex than models A and B, there was a need to make certain comparisons between the three. Because both model C and model A featured fluxes of zero out of the device top and bottom, it made the most sense to compare these two directly as seen below in Figure 5.5.2.

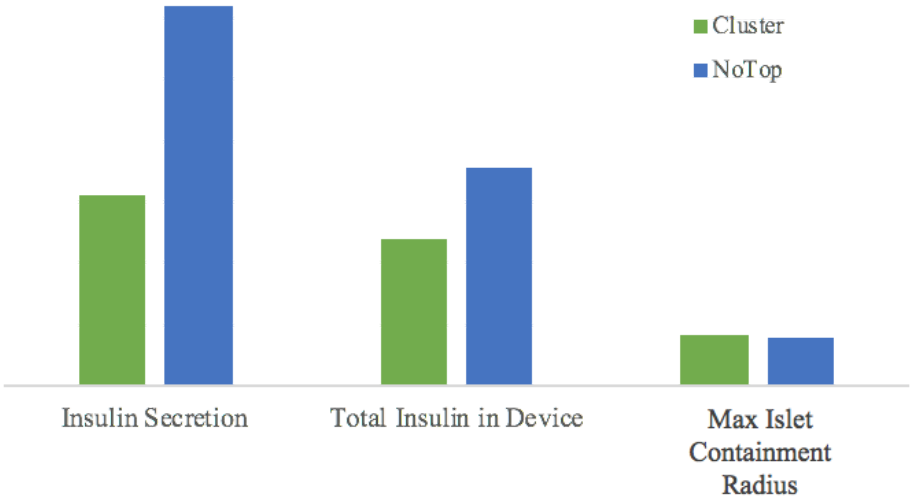

Figure 5.5.2 (C, A): *Bar graph comparison of Model C and Model A*. Measurements are for insulin secretion, total insulin in the device, and the max radius of the islet cell containment. The insulin secretion ($(mol \cdot m^{-2}s^{-1})$) is measured is displayed at a factor of 10^{-12}, total insulin in the device ($mol \cdot m^{-3}$) is displayed at a factor of 10^{-11}, and max width of islet cell containment solution is measured in millimeters.

Particularly, models A and C were compared directly since both had no oxygen flux entering from the caps of the device, as illustrated in Figure 5.5.2. Even at similar widths, model C produced and secreted less insulin since less cells were properly exposed to oxygen. Regardless, the two schematics produced similar concentrations of insulin and secreted a similar amount of insulin (both within an order of magnitude), as shown in Figure 5.5.2. Therefore, the conclusion could be made that the physical approximation made throughout this report did alter the insulin fluxes reported, but the trends shown by these data points are sufficient enough to simplify the model into a two dimensional axisymmetric model.

Upon completion of studies which accumulated results and data for all three of the models (A, B, C), the next step involved plotting the results in order to generate a comparison across all three of the models that were created in the computational modeling processes. Looking specifically at insulin flux as one of the most significant components of the devices, Figure 5.5.3 below reveals the impact of incorporating each of the three models on the insulin flux of an encapsulation device.

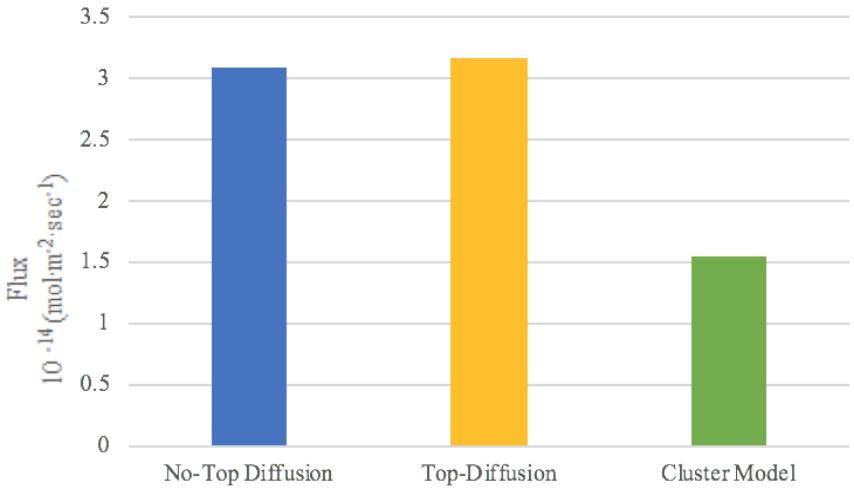

Figure 5.5.3 (A, B, C): *Total insulin flux for Models A, B, and C.* The total insulin flux of each of the models is generated through summing calculated fluxes at the upper cut line and height cut along the axis.

What may be understood by these results is that while variation in insulin flux between the Top-Diffusion and No-Top Diffusion models are only slight, both of these models were found to generate much larger values of Insulin Flux than the Cluster Model. The calculated flux of the Top-Diffusion was determined to be the highest overall at $3.17 \cdot 10^{-14}$ $(mol \cdot m^{-2}s^{-1})$, and that of the No-Top Diffusion was slightly lower at $3.09 \cdot 10^{-14}$ $(mol \cdot m^{-2}s^{-1})$. The value of insulin flux calculated for the cluster model in comparison came to be significantly lower than the flux values of the other two models at $1.55 \cdot 10^{-14}$ $(mol \cdot m^{-2}s^{-1})$. The clusters here were modeled as an extreme form of cluster integration in which the cluster sizes were too large to allow sufficient oxygen concentrations to be maintained within the cluster interiors to keep all of the cells alive. The purpose of using this larger-than-actual cluster sizing was to emphasize the importance of identifying an intermediate between total uniform islet cell incorporation (as was done in Models A and B), and cluster integration with sizes too large for total cell survival.

5.6 Sensitivity Analysis

A sensitivity analysis was performed to ensure these models were built with regards to the model's capabilities over a range of parameters, uncertainties in input parameters are visualized, and optimization may be carried out. By adjusting particular parameters by different percentages, one is able to determine the degree of accuracy needed of that particular input; i.e. the more sensitive the insulin concentration is to that parameter, the more accurate that parameter needs to be in the model.

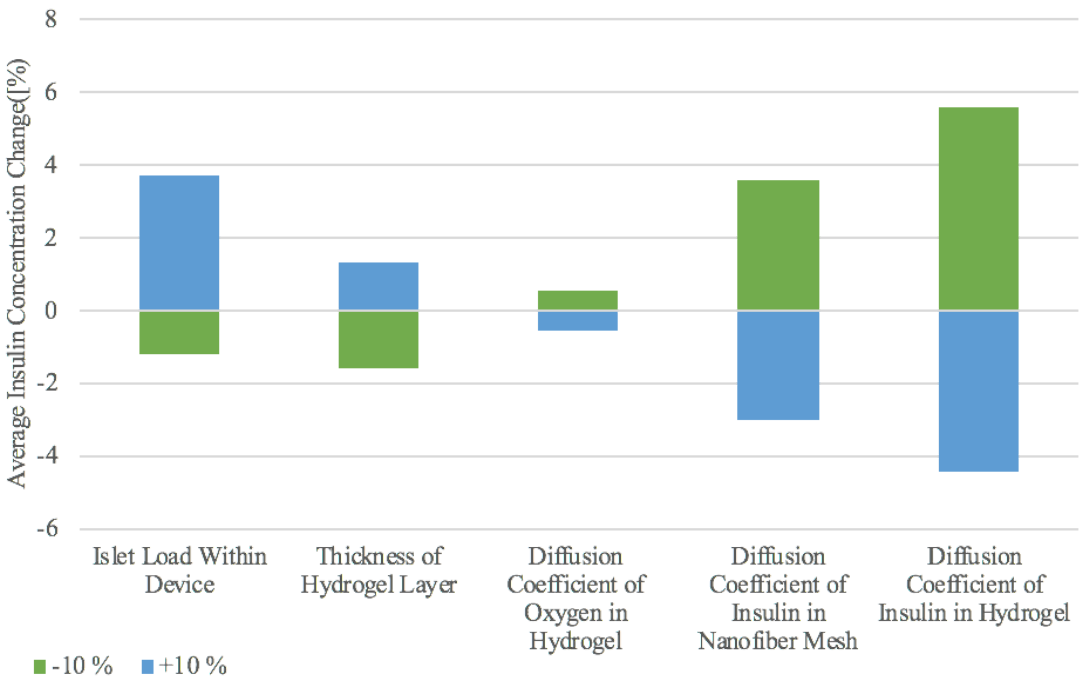

Figure 5.6.1 (B): Sensitivity analysis performed varying +/- 10 percent of parameters chosen to analyze effect on the percent change of average insulin concentration. Islet load, thickness of hydrogel, diffusion coefficient of oxygen in hydrogel, as well as diffusion coefficients of insulin in nanofiber mesh and hydrogel were all tested.

The change in average insulin concentration after varying the amount of islet loading within the device is in accordance with the trend that as the islet load increases the insulin secretion of the device decreases; therefore, a larger change in concentration of insulin would occur within the device if islet load increases. Varying the hydrogel layer thickness would cause more molecules of insulin to be present within that portion of that hydrogel, thus altering the insulin concentration within the device. Altering the diffusion coefficient of both oxygen and insulin showed the same inverse relationship to change in insulin concentration throughout the device. As the diffusion coefficient decreases, it takes much longer for insulin molecules to travel across the nanofibrous and hydrogel layers for a longer period of time, effectively increasing the insulin concentration, as less insulin is able to leave the device [13].

This device was most sensitive to the change in diffusivity coefficients of insulin in both the nanofiber mesh and hydrogel. The next most sensitive parameter was islet load, which one can revisit to ensure the appropriate islet density is present for the desired amount of insulin production. There is a direct relationship for the diffusion of oxygen within the hydrogel layer and insulin production because as more oxygen enters the device, more cells are able to produce insulin. Furthermore, as the thickness of impeding layers of hydrogel and nanofiber mesh are increased, less oxygen enters the device and results in cell death due to hypoxia.

5.7 Mesh Convergences

Mesh - A

The complete mesh implemented for A (No-Top Diffusion Model) may be seen below in Figure 5.7.1. The mesh constructed consisted of 76878 elements with 8308 boundary elements and featured 148444 degrees of freedom.

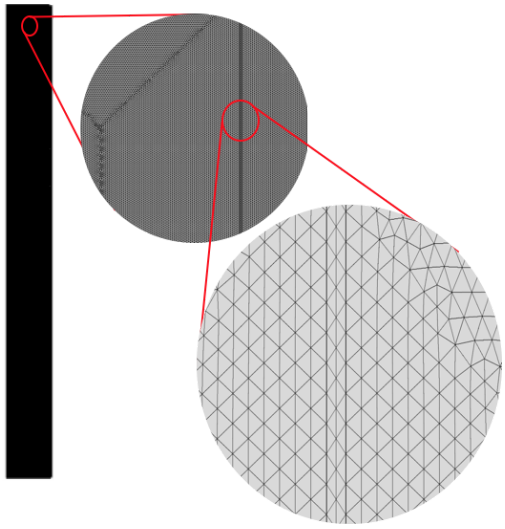

Figure 5.7.1 (A): Mesh plot of No-Top Diffusion model with magnifications revealing mesh close-up and domain boundaries.

Mesh - B

The complete mesh implemented for B (Top Diffusion Model) may be seen below in Figure 5.7.2. The mesh constructed consisted of 63362 domain elements and 2624 boundary elements, and featured 161544 degrees of freedom.

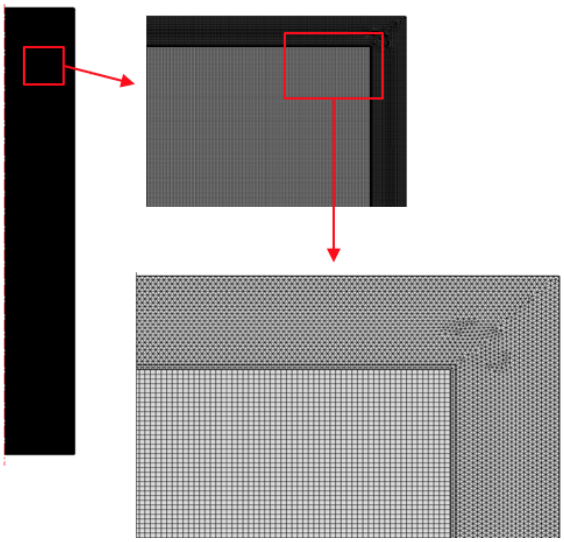

Figure 5.7.2 (B): Mesh plot of top diffusion model with magnifications revealing mesh close-up and domain boundaries. The mesh implemented is much finer in the confinement areas.

Mesh - C

The complete mesh implemented for C (Cluster Model) may be seen below in Figure 5.7.3. The mesh constructed consisted of 290297 domain elements, 38104 boundary elements, and 1983 edge elements. The number of degrees solved for was 165270.

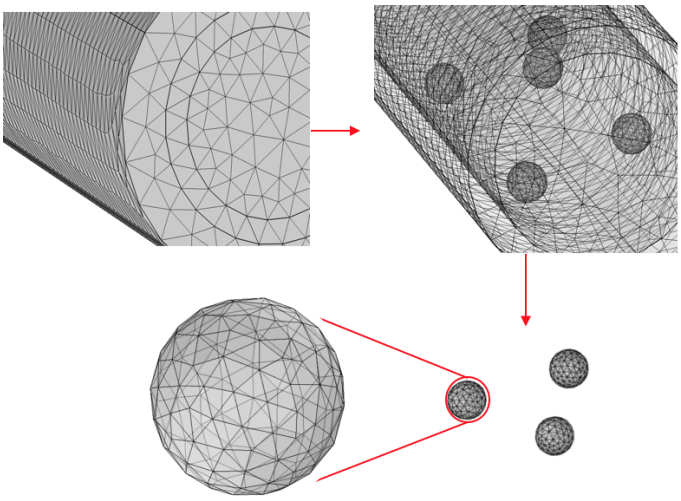

Figure 5.7.3 (C): Mesh plot of cluster model with magnifications revealing mesh close-up and inner islet cell clusters.

Mesh Convergence Plot

In order to ensure that the three models created had minimal discretization error spatially, mesh convergences were performed across each model as seen below in Figure 5.7.4.

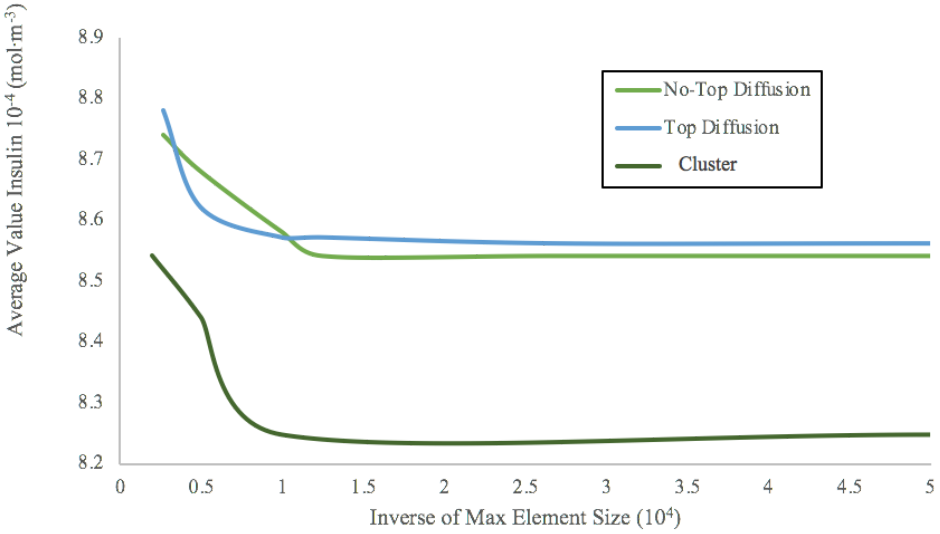

Figure 5.7.4 (A,B,C): *Mesh convergence plot of inverse of maximum element size vs average insulin concentration inside devices.* Each of the models on which the mesh convergence had been performed converged around similar values for the inverse of max element size.

In order to assure true convergence was reached with regards to the results of the models, a parametric sweep was run with the maximum element size being refined further and further until the insulin concentration at the points shown below for each schematic (Figure 5.7.5) no longer changed with refining the maximum element size. The points were specifically chosen as they are representative of points with large concentration gradients of insulin. Minimization of discretization error was maximized at these points for mesh convergence in order. Despite the maximum x-axis value being set as $5 \cdot 10^{4,}$ the mesh convergence was carried out up to value of $15 \cdot 10^4$ to ensure proper convergence.

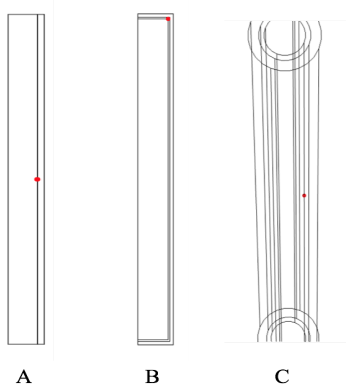

Figure 5.7.5 (A,B,C): *Mesh convergence points.* Red colored points represent points in three models at which mesh convergence performed on level of insulin concentration. Points chosen are representative of area where large concentration gradients may be.

5.8 Validation

The process of validating the study and the results generated was performed over two steps. Initially, the role of oxygen in modulation of insulin was validated through comparing the data obtained to experimental data from [27] paper which involved a similar study performed experimentally in mice. Data was taken from islets similarly encapsulated within an alginate-based hydrogel, insulin secretion was sampled as a function of this partial pressure as the islets were exposed to varying partial pressures of oxygen. The model generated in this study reveal correspondences and similarities to the experimental data obtained, as can be seen below in Figure 5.8.1. The small divergence from the computational data may be explained because [27] only encapsulated singular islets with alginate, as opposed to our model which encapsulated a large number of islets within one containment core.

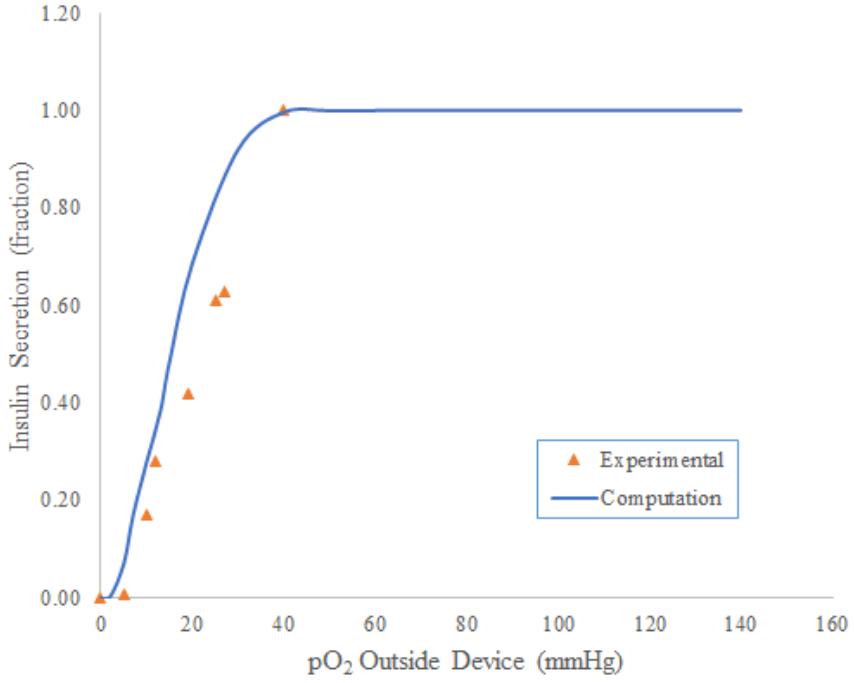

Figure 5.8.1: *Validation of insulin secretion.* Fractions of insulin secretion were plotted in response to partial pressure of oxygen. The experimental solutions [source] generated through creating a similar device implemented in a mouse model are compared to the results obtained from the computational models generated.

Next, validation was pursued with regards to significant physical approximations established in the creation of a model with clusters. Model C was compared to Model A, and the two revealed results comparable to each other, as shown previously in Figure 5.5.2. This trend allowed the model to approximate a complex 3D problem as a simpler 1D problem in which the islets were modeled as homogeneously distributed within the islet cell containment core. Note the parameter when compared across schematics generates results that are within the same order of magnitude.

DuLong, Buchwald, An, and Su have closely studied the feasibility and functionality of cell encapsulation devices for the treatment of Type 1 Diabetes [9-10,18,21-23]. Making use of their prior findings, this study enabled a more thorough review of the device's capabilities and modularity through the development of computational modeling programs. Such models allow for different researchers to, for example, test out different parameters within an accurate model in the body prior to surgically inserting such a device such as the optimum thickness of gels for glucose/oxygen sensing and insulin production [21]. These values have been examined through an analysis on oxygen, insulin, and glucose concentrations across the domain. The main parameter focus in this study due to its role as somewhat of a limiting molecule, was oxygen. The way this study modeled concentrational uptake of oxygen into the cells to determine the amount of islets hat survive is validated by DuLong, Buchwald, and Dr. Ma's Lab, as oxygen is the main parameter in controlling insulin production [23,28]. Furthermore, by placing the cells at their max size possible, we were able to determine the critical radius, i.e. the max radius the cells can reach to ensure least amount of necrosis occurs [24,28].

6. Conclusion

In this study, we used computer simulations to simulate the transfer of oxygen, glucose and insulin across the nanofiber matrix and hydrogel layer to analyze diffusion as well as production of insulin through the outermost membrane of this device. In doing so, this process will allow us to observe the effects of glucose and oxygen availability on insulin production. The process involves two major transfers: 1) Influx of glucose and oxygen into the cells, and 2) release of insulin out of the matrix and into the body. By analyzing these processes through the development of three models on COMSOL, we can alter and optimize the parameters of the hydrogel as well as the material makeup to optimize the functionality of this device for treating Type 1 Diabetes.

Cell encapsulation as a treatment for diabetes is a desirable substitute to common invasive and tedious treatments for Type 1 Diabetes. This report studied the effects of particular parameters on insulin production in three pseudo steady state models immediately after eating a meal. From these computational results, this study revealed that the width of the nylon saturated nanofiber matrix should be minimized for maximal insulin secretion, however, this layer can not be less than a certain threshold, as the nylon layer is necessary for fidelity of the device within the harsh environments of the peritoneal cavity [10]. Further,

islet loading must be decreased in order to maximize the insulin secretion. However, this would mean creating a wider device that would make implantation and/or retrieval of this device from a patient's peritoneal cavity much more surgically invasive.

A hydrogel composed of gelatin would improve the amount of cells this device could support, and thus increase insulin produced/secreted. This device should also have ends that are open to diffusion to occur both radially and across the z-axis, as this increases insulin secretion with no harsh side effects for the patient. While this device might be able to treat Type 1 Diabetes when implanted within a mouse, the amount of insulin that this device supplies to the body is far from the amounts necessary for humans with Type 1 Diabetes. Therefore, by optimizing parameters of this device as suggested throughout this report can lead to a desired production of insulin so this treatment can be applicable in humans. At steady state, glucose is relatively constant, thus during and shortly after a meal, insulin is not modulated by blood sugar. However, to further enhance this study, research can look at cellular response to glucose spikes following a meal and the production of insulin from the device into the patient(s) in relation to time.

7. Future Improvements

Design considerations as they pertain to the information revealed by this study involve the choice of specific parameters to allow for increased cell survival, larger critical radii, and increased insulin flux. This study recommends that in choosing hydrogels for encapsulation methods, when working with biological mechanisms which require oxygen, gelatin may be a tremendously suitable choice because of the relatively high solubility of oxygen coefficient it has. This high oxygen solubility allows for the gelatin to hold onto oxygen molecules better than other hydrogels might, and therefore the cells incorporated in these devices would have better access to oxygen. Another design consideration has to do with the thicknesses of the nanofibers mesh layers incorporated into the devices. While added volume to confinement layers may seem to obviously work against the purposes of these devices, variations in nylon mesh layer thickness were showed to have little impact on the insulin secreting capabilities of these devices. As multidirectional methods of transfer were also considered in comparison to single direction transfer models, the impact of incorporating more surfaces through which chemical species transfers could occur was very beneficial to the life of the device with regards to its access to oxygen and ability to secrete insulin. As these aspects of the confinement were considered and studied, so were aspects of the actual containment layer itself considered. In varying the amounts and forms by which islet cells are incorporated into cellular encapsulation devices, the impact of the means by which the addition of these cells are added may be noted. Larger clusters of islet cells seem to quickly reach necrosis and die due to a lack of oxygen. More dispersed and larger devices may be a solution. In keeping the same parameters, a future improvement to the study may involve incorporating an objective function to fully optimize the model across the set of all parameters.

Several additional parameters with potential to greatly impact the efficiency and efficacy of the model may be considered more closely in future projects and future improvements to the technology. One such means by which the system may be improved is through accounting for cell growth within the device. Cells within the core of cell-encapsulation devices require a particular amount of oxygen and other nutrients to continue to grow. As the stem cells within the matrix begin to grow, the matrix which contains

the islet cells may also expand, causing the thinning of walls, widening of pores, and tremendous potential for structural damage. In order to better understand these mechanisms, a potential future approach may be to look into the impacts of Young's modulus and elasticity as they pertain to this cell growth and expansion. Furthermore, this increases the likelihood that cells within the islet containment will be able to escape from the device and potentially lead to the development of tumors elsewhere. Even greater is the concern immune cells will travel inside, also shortening the life of the device/increasing harm to the patient.

The potential for immune responses attacking the islet cells in the encapsulation device is an area of future improvement that may also be duly considered. This is an issue that needs to be further analyzed. Inflammatory factors are still able to freely diffuse into the hydrogel and damage the encapsulated cells [18], and further, simply modeling this as a diffusion problem neglects to account for this factor in the peritoneum. Need to combat the cellular reaction carried around the device such as the initiation of fibrosis which occurs as a response of the immune system attaching foreign bodies. Fibroblasts begin to cover and accumulate over the foreign objects introduced to the body, and over time and eventually completely block off chemical species transfer which would be a large problem considering the ways in which the device works. In order for these devices to work continuously, the issue of fibrosis must be swiftly avoided [10].

8. Appendix A – Input Parameters

Table 4: *Input Parameters*

Parameter	Symbol	Value	Source
Concentration Glucose Outermost Boundary (Hydrogel) (mM)	C_{Gh}	$K_g \cdot C_{go}$	[15]
Concentration Oxygen Outermost Boundary (Hydrogel) (mM)	C_{Oh}	$\alpha_{alginate} \cdot P_o$	[15]
Critical Oxygen Concentration (mM)	C_{cr}	0.001	[7]
Diffusivity of Glucose in Alginate ($m^2 s^-$)	$D_{G\ Alg}$	$0.6 \cdot 10^{-9}$	[9]
Diffusivity of Glucose in Containment ($m^2 s^-$)	$D_{G\ ECM}$	$5.5 \cdot 10^{-9}$	[9]
Diffusivity of Glucose in Nanofiber Mesh (Nylon) ($m^2 s^{-1}$)	$D_{G\ N}$	$0.6 \cdot 10^{-9}$	[18]
Diffusivity of Insulin Alginate ($m^2 s^{-1}$)	$D_{i\ Alg}$	$0.1 \cdot 10^{-9}$	[9]
Diffusivity of Insulin in Containment ($m^2 s^-$)	$D_{i\ ECM}$	$0.0955 \cdot 10^{-9}$	[9]
Diffusivity of Insulin in Nanofibers (Nylon) ($m^2 s^-$)	D_{in}	$0.609 \cdot 10^{-10}$	[17]
Diffusivity of Oxygen in Alginate ($m^2 s^{-1}$)	D_{O2Alg}	$2.5 \cdot 10^{-9}$	[9]
Diffusivity of Oxygen in Containment ($m^2 s^{-1}$)	D_{O2ECM}	$2.45 \cdot 10^{-9}$	[9]

Parameter	Symbol	Value	Source
Diffusivity of Oxygen within Nanofiber mesh (Nylon) ($m^2 s^{-1}$)	D_{O2N}	$2.5 \cdot 10^{-9}$	[17]
Glucose Concentration Outside (mM)	C_{GO}	11.11	[10]
Glucose Reaction (Degradation) (mol $m^{-3}s^{-1}$)	r_g	$MM_{GG}(C_o)$	[9]
Half-Maximal Glucose Concentration Modulating Glucose Consumption (mM)	K_{GG}	6	[9]
Half-Maximal Oxygen Concentration Modulating Insulin Consumption (mM)	K_{O2i}	0.003	[9]
Half-Maximal Oxygen Concentration Modulating Oxygen Consumption (mM)	K_{O2O2}	$1 \cdot 10^{-3}$	[9]
Height of Device (mm)	h	20	[10]
Hill function coefficient	n	3	[9]
Hydrogel Thickness (mm)	t_h	0.15	[10]
Insulin Reaction (Production) (mol $m^{-3}s^{-1}$)	r_i	$MM_{o2\ ins}(C_o)$	[9]
Islet Cell (ECM) Radius (mm)	t_r	0.49-2.12 [mm]	
Islet Load (Volume Fraction)	z	0.005-0.04	
Michaelis Menten Glucose and Glucose (mM s^-)	MM_{GG}	$\frac{x \cdot V_{max\,G}}{x+K_{GG}}$	[9]
Michaelis Menten O_2 and Insulin (mM s^-)	MM_{O2ins}	$\frac{x^n \cdot V_{max\,ins}}{x^n+K_{o_2ins}^{\ n}}$	[9]
Michaelis Menten O_2 and O_2 (mM s^-)	MM_{O2O2}	$\frac{x \cdot V_{max\,O_2}}{x+K_{O_2O_2}}$	[9]
Nanofiber Matrix Thickness (mm)	t_n	0.01-.25	
Oxygen Reaction (Removal) (mol $m^{-3}s^{-1}$)	r_o	$MM_{O2O2}(C_o)$	[9]
Oxygen Solubility in Alginate (mM Pa^-)	$\alpha_{alginate}$	$9.3 \cdot 10^{-6}$	[15]
Oxygen Solubility in Fibrin (mM Pa^-)	α_{fibrin}	$9.75 \cdot 10^{-6}$	[13]
Oxygen Solubility in Gelatin	$\alpha_{gelatin}$	$1.38 \cdot 10^{-5}$	[11]
Partial Pressure of Oxygen in Alginate (mmHg)	P_o	40	[8]
Partition Coefficient for Glucose in Water and Alginate	K_g	0.95	[15]

Parameter	Symbol	Value	Source
Smoothing Constant for Heaviside Function	s	$5 \cdot 10^{-5}$	[15]
Temperature (K)	T	310.15	[3]
V_{max} Glucose (mM s^{-})	$V_{max\ G}$	0.028	[18]
V_{max} Insulin (mM s^{-})	$V_{max\ i}$	$3 \cdot 10^{-5}$	[18]
V_{max} Oxygen (mM s^{-})	$V_{max\ O2}$	0.034	[18]

9. Appendix B – Mathematical Methods

A - No-Top Diffusion Model $$D_j[\frac{1}{r}\frac{\partial}{\partial r}(r\frac{\partial c_j}{\partial r})] + r_j = 0 \quad (1)$$

B - Top-Diffusion Model $$D_j[\frac{1}{r}\frac{\partial}{\partial r}(r\frac{\partial c_j}{\partial r}) + (\frac{\partial^2 c_j}{\partial z^2})] + r_j = 0 \quad (2)$$

C - Clusters Model $$D_j[\frac{1}{r}\frac{\partial}{\partial r}(r\frac{\partial c_j}{\partial r}) + \frac{1}{r^2}(\frac{\partial^2 c_j}{\partial \theta^2}) + (\frac{\partial^2 c_j}{\partial z^2})\ ] + r_j = 0 \quad (3)$$

9.1 Insulin Diffusivity in Nanofiber Mesh

The following obstruction model was implemented in this study in order to determine the diffusivity of insulin in nylon. This model specifically describes the distribution of openings between randomly oriented 6,6 polyamide nylon fibers impregnated with hydrogel.

$$\frac{D_{in}}{D_{i,water}} = exp[-\frac{\pi}{4}(\frac{r_s+r_f}{r_p+r_f})^2] \quad (4)$$

Where D_{in} is the diffusivity of insulin within the nylon layer, D_{iAlg} is the diffusivity within the hydrogel layer, r_s is the radius of the solute that is being analyzed (insulin hydrodynamic radius) [22] , r_f is the radius of the polymer (average radius of the nylon fibers) and r_p is the radius of the pores within the nylon layer.

$$\frac{D_{in}}{10^{-10}} = exp[-\frac{\pi}{4}(\frac{5.6\cdot 10^{-6}m+200\cdot 10^{-9}m}{10^{-6}m+200\cdot 10^{-9}m})^2] \quad (5)$$

(note that 10^{-10} is the diffusivity of insulin within water)

$D_{in} = 0.609 \cdot 10^{-10}$

9.2 Young Modulus Layer Consideration

Where a_n 's are the volume fraction of each individual layer and E_n are the Young's moduli of each respective layer - An $E = a_1E_1 + a_2E_2$ (6)

9.3 Glucose Concentration at Hydrogel Layer

$$C_{Gh} = C_{Go} \cdot K_G \quad (7)$$
$$= 0.95 \cdot 11.11\,(\text{mM})$$
$$= 10.49\,(\text{mM})$$

9.4 Oxygen Concentration at Hydrogel Layer

$$C_{Oh} = \alpha_{alginate} \cdot P_O \quad (8)$$
$$= 9.3 \cdot 10^{-6}\ (\text{mM} \cdot \text{Pa}^{-1}) \cdot 40\ (\text{mmHg}) \cdot 133.33\ (\text{Pa} \cdot \text{mmHg}^{-1})$$
$$= .0496\,(\text{mM})$$

9.5 Sufficient Oxygen Concentration

$$C_O = C_{O,effective}$$
$$= C_O - C_{cr} \quad (9)$$

10. Appendix C – Experimental Setup

10.1 Electrospinning Mechanism

The following mechanism is a mockup visual of what the electrospinning aspect of the experimental setup of developing the nanofiber (nylon) mesh layer might entail.

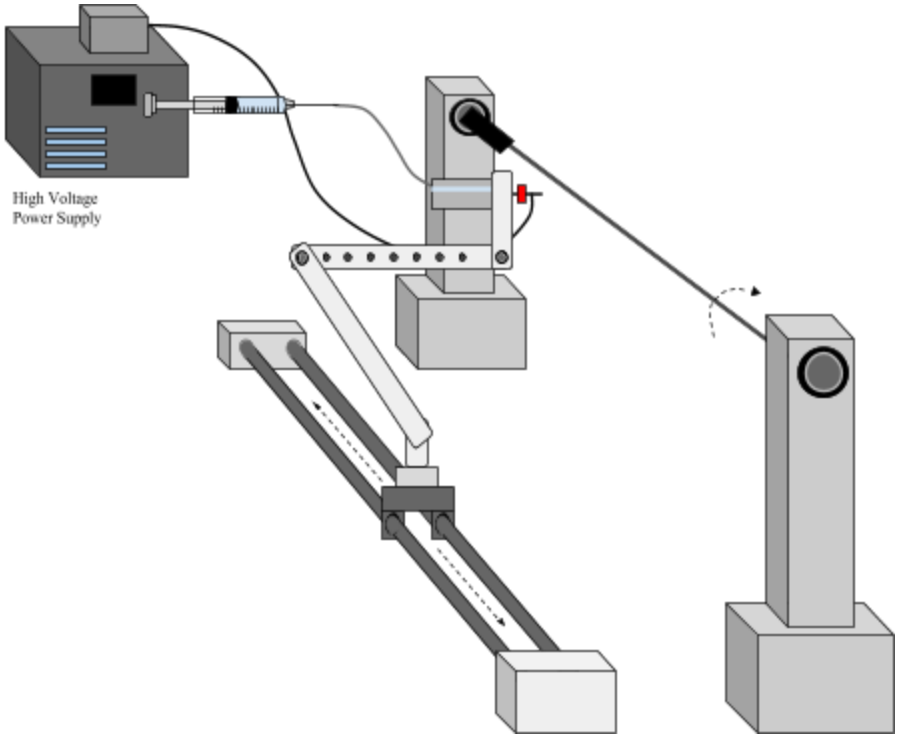

Figure 10.1.1*: Electrospinning mechanism schematic*. Device would be used in order to develop nanofiber layer surrounding islet cell containment, and surrounded by hydrogel layer of cell encapsulation device.

11. Appendix D - CPU and Memory Usage

Table 3: CPU and Memory Usage of Files

Schematic	Virtual Memory	Real Memory	CPU
A	2.82 GB	2.32 GB	219s
B	2.59 GB	3.44 GB	176s
C	1.81 GB	1.97 GB	10s

12. Appendix E - COMSOL Contours

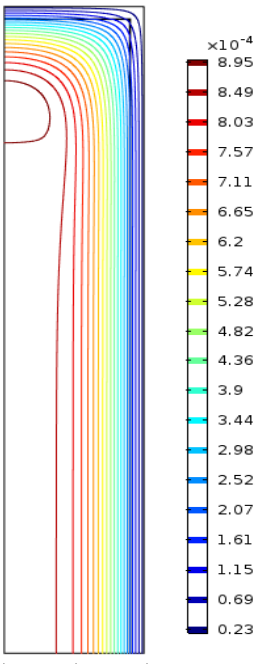

Figure 12.1: *Contour Lines of Insulin Concentrations.* Since schematic B has variation of insulin both in the r-axis as well as the z-axis, a graph of insulin concentration across a straight line through the device will not show the true concentration profile present within the device. The contour plot present shows different concentrations present within the device.

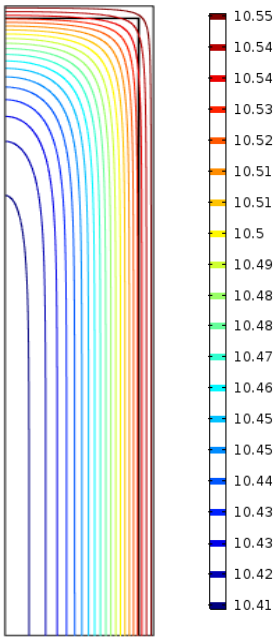

Figure 12.2: *Glucose Concentrations Shown Through Contour Lines.* Due to the same issue as with insulin concentrations, the concentration of profile will also vary in both the r and z directions, therefore a graph does not have the capability of effectively showing the concentration profile. Note on this contour that the concentration of glucose does not vary a lot throughout the device. This justifies our decision to

not include modulation of insulin by glucose concentration but rather assume that the concentration is nearly constant and not cause varying secretions of insulin due to its change in concentration.

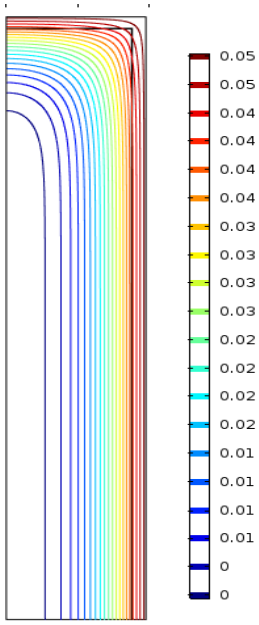

Figure 12.3: *Oxygen Concentration Shown Through Contour Lines.* Again, contour lines are the method of choice for the team to model species within this device due to the multiaxial diffusion. Note in this contour plot how close oxygen approaches to a critical concentration (See Table 4 in Appendix A). The critical concentration of oxygen is the absolute minimum concentration necessary to sustain cell life. In order to generate this kind of profile our team optimized the radius of the extracellular matrix so that the furthest point from any boundary saturated with oxygen (shown at 0,0) will have enough oxygen. The optimization data is shown below.

References:

[1] Devendra, Devasenan et al. “Immunologic endocrine disorders,” *Journal of Allergy and Clinical Immunology*, Vol 111 , Issue 2 , S624 - S636

[2] Morley, John E. “Overview of Endocrine Disorders - Endocrine and Metabolic Disorders.”*Merck Manuals Professional Edition*, Aug. 2016,

[3] “What Is Diabetes?” *National Institute of Diabetes and Digestive and Kidney Diseases*, U.S. Department of Health and Human Services, 1 Nov. 2016,

[4] Brutsaert, Erika F. “Hypoglycemia - Hormonal and Metabolic Disorders.” *Merck Manuals Consumer Version*, Aug. 2016,

[5] Fokkert, M J, et al. “Performance of the FreeStyle Libre Flash Glucose Monitoring System in Patients with Type 1 and 2 Diabetes Mellitus.” *BMJ Open Diabetes Research & Care*, BMJ Specialist Journals, 1 Feb. 2017, drc.bmj.com/content/5/1/e000320.

[6] Voltarelli JC, et al.. Autologous Nonmyeloablative Hematopoietic Stem Cell Transplantation in Newly Diagnosed Type 1 Diabetes Mellitus. *JAMA.* 2007;297(14):1568–1576.

[7] J.-L. Dulong and C. Legallais, “A theoretical study of oxygen transfer including cell necrosis

for the design of a bioartificial pancreas," *Biotechnology and Bioengineering*, vol. 96, no. 5, pp. 990–998, 2007.

[8] Flessner, Michael. "Peritoneal Transport Physiology: Insights from Basic Research." *Journal of the American Society of Nephrology*, 1 Aug. 1991, jasn.asnjournals.org/content/2/2/122.long.

[9] P. Buchwald, A. Tamayo-Garcia, V. Manzoli, A. A. Tomei, and C. L. Stabler, "Glucose-stimulated insulin release: Parallel perifusion studies of free and hydrogel encapsulated human pancreatic islets," *Biotechnology and Bioengineering*, vol. 115, no. 1, pp. 232–245, 2017.

[10] D. An, et al. "Developing robust, hydrogel-based, nanofiber-enabled encapsulation devices (NEEDs) for cell therapies," *Biomaterials*, vol. 37, pp. 40–48, 2015.

[11] E. Chaix, C. Guillaume, and V. Guillard, "Oxygen and Carbon Dioxide Solubility and Diffusivity in Solid Food Matrices: A Review of Past and Current Knowledge," Comprehensive Reviews in Food Science and Food Safety, vol. 13, no. 3, pp. 261–286, 2014.

[12] M. T. Novak, F. Yuan, and W. M. Reichert, "Macrophage embedded fibrin gels: An in vitro platform for assessing inflammation effects on implantable glucose sensors," *Biomaterials*, vol. 35, no. 36, pp. 9563–9572, 2014.

[13] G. N. Ling, "Permeability," *In Search of the Physical Basis of Life*, pp. 377–436, 1984.

[14] S. M. Ehsan and S. C. George, "Nonsteady State Oxygen Transport in Engineered Tissue: Implications for Design," *Tissue Engineering Part A*, vol. 19, no. 11-12, pp. 1433–1442, 2013.

[15] A. Ernst. Personal Lecture, Topic: "Hydrogel Encapsulation Computational Model Seminar". School of Biological Engineering, Cornell University, Ithaca, NY, Feb., 24, 2018.

[16] S. Hvidt, "Insulin association in neutral solutions studied by light scattering," Biophysical Chemistry, vol. 39, no. 2, pp. 205–213, 1991.

[17] B. Amsden, "An Obstruction-Scaling Model for Diffusion in Homogeneous Hydrogels," *Macromolecules*, vol. 32, no. 3, pp. 874–879, 1999.

[18] P. Buchwald, "FEM-based oxygen consumption and cell viability models for avascular pancreatic islets," *Theoretical Biology and Medical Modelling*, vol. 6, no. 1, p. 5, 2009.

[19] J. V. Nauman, P. G. Campbell, F. Lanni, and J. L. Anderson, "Diffusion of Insulin-Like Growth Factor-I and Ribonuclease through Fibrin Gels," *Biophysical Journal*, vol. 92, no. 12, pp. 4444–4450, 2007.

[20] K. Bhunia, S. S. Sablani, J. Tang, and B. Rasco, "Non-invasive measurement of oxygen diffusion in model foods," *Food Research International*, vol. 89, pp. 161–168, 2016.

[21] Su, Jing, et al. "Anti-Inflammatory Peptide-Functionalized Hydrogels for Insulin-Secreting Cell Encapsulation." *Egyptian Journal of Medical Human Genetics*, Elsevier, 25 Sept. 2009, www.sciencedirect.com/science/article/pii/S0142961209009752.

[22] B. B. Benson and D. Krause, "The concentration and isotopic fractionation of oxygen dissolved in freshwater and seawater in equilibrium with the atmosphere," Limnology and Oceanography, vol. 29, no. 3, pp. 620–632, 1984.

[23] R. A. Bader, K. T. Herzog, and W. J. Kao, "A study of diffusion in poly(ethyleneglycol)-gelatin based semi-interpenetrating networks for use in wound healing," *Polymer Bulletin*, vol. 62, no. 3, pp. 381–389, 2008.

[24] M. Ahearne, Y. Yang, A. J. E. Haj, K. Y. Then, and K.-K. Liu, "Characterizing the viscoelastic properties of thin hydrogel-based constructs for tissue engineering applications," Journal of The

Royal Society Interface, vol. 2, no. 5, pp. 455–463, 2005.
[25] "MatWeb - The Online Materials Information Resource," Overview of materials for Polycarbonate, Extruded. [Online].
[26] Fairbanks, D. F., and C. R. Wilke. "Diffusion Coefficients in Multicomponent Gas Mixtures," *University of California, Berkeley*, 5 July 1949.
[27] K. E. Dionne, C. K. Colton, and M. L. Yarmush, "Effect of Oxygen on Isolated Pancreatic Tissue," ASAIO Journal, vol. 35, no. 3, pp. 739–741, 1989.
[28] Buchwald, P. "A Local Glucose-and Oxygen Concentration-Based Insulin Secretion Model for Pancreatic Islets." *Advances in Pediatrics.*, U.S. National Library of Medicine, 21 June 2011.

Team member name	Nicole Alimena	Edward Bao	Tigran Mehrabyan	Kaavian Shariati	NOT DONE
Wrote abstract	x			x	
Edited abstract		x	x	x	
Wrote introduction	x			x	
Edited introduction	x			x	
Wrote method section	x		x	x	
Edited method section	x		x	x	
Wrote results section	x		x	x	
Edited results section	x		x	x	
Wrote discussion section	x		x	x	
Edited discussion section	x		x		
Wrote summary and conclusion section	x		x	x	
Edited summary and conclusion section	x		x	x	
Wrote bibliography section		x			
Edited bibliography section		x			
Prepared processed data table for appendix	x	x	x	x	
Checked data in processed data table in appendix	x	x	x	x	
Prepared figures or tables for main text	x	x	x	x	
Checked figures or tables in main text	x		x	x	
Assigned tasks to group members				x	
Put the report together from the parts provided by others	x		x	x	
Read and edited entire document to check for consistency	x			x	